

University of Montana

## ScholarWorks at University of Montana

---

Graduate Student Theses, Dissertations, &  
Professional Papers

Graduate School

---

2006

### The influence of glacial erosion on landscape evolution and basin morphology in the Bitterroot Mountains Montana

Shawn Naylor

*The University of Montana*

Follow this and additional works at: <https://scholarworks.umt.edu/etd>

**Let us know how access to this document benefits you.**

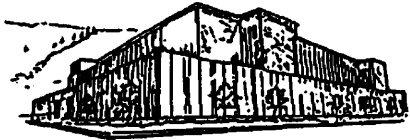
---

#### Recommended Citation

Naylor, Shawn, "The influence of glacial erosion on landscape evolution and basin morphology in the Bitterroot Mountains Montana" (2006). *Graduate Student Theses, Dissertations, & Professional Papers*. 8281.

<https://scholarworks.umt.edu/etd/8281>

This Thesis is brought to you for free and open access by the Graduate School at ScholarWorks at University of Montana. It has been accepted for inclusion in Graduate Student Theses, Dissertations, & Professional Papers by an authorized administrator of ScholarWorks at University of Montana. For more information, please contact [scholarworks@mso.umt.edu](mailto:scholarworks@mso.umt.edu).



Maureen and Mike  
**MANSFIELD LIBRARY**

The University of  
**Montana**

---

Permission is granted by the author to reproduce this material in its entirety, provided that this material is used for scholarly purposes and is properly cited in published works and reports.

**\*\*Please check "Yes" or "No" and provide signature\*\***

Yes, I grant permission

No, I do not grant permission

Author's Signature: SL MR

Date: 5/30/06

Any copying for commercial purposes or financial gain may be undertaken only with the author's explicit consent.

---



THE INFLUENCE OF GLACIAL EROSION ON LANDSCAPE  
EVOLUTION AND BASIN MORPHOLOGY IN THE  
BITTERROOT MOUNTAINS, MONTANA

by

Shawn Naylor

B.S., Indiana University, Bloomington, Indiana, 2001

Presented in partial fulfillment of the  
requirements for the degree of

Master of Science

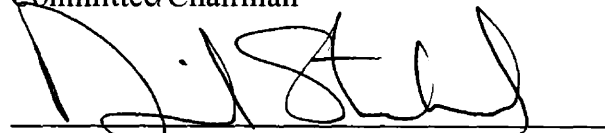
The University of Montana

May 2006

Approved by:



\_\_\_\_\_  
Committee Chairman



\_\_\_\_\_  
Dean, Graduate School

30 May 2006

\_\_\_\_\_  
Date



UMI Number: EP39082

All rights reserved

INFORMATION TO ALL USERS

The quality of this reproduction is dependent upon the quality of the copy submitted.

In the unlikely event that the author did not send a complete manuscript and there are missing pages, these will be noted. Also, if material had to be removed, a note will indicate the deletion.



UMI EP39082

Published by ProQuest LLC (2013). Copyright in the Dissertation held by the Author.

Microform Edition © ProQuest LLC.

All rights reserved. This work is protected against  
unauthorized copying under Title 17, United States Code



ProQuest LLC.  
789 East Eisenhower Parkway  
P.O. Box 1346  
Ann Arbor, MI 48106 - 1346

## The Influence of Glacial Erosion on Landscape Evolution and Basin Morphology in the Bitterroot Mountains, Montana

Committee Chairman: Emmanuel Gabet



The efficiency of glacial erosion compared to nonglacial processes has long been debated with most researchers acknowledging that glacial denudation exceeds even the most active fluvial systems. Constraining the relative efficiency of glacial erosion is vital to improving our understanding of alpine landscape evolution, but difficult because 1) erosional processes typically overlap in space and time and 2) comparisons must be made with uniform lithology and precipitation. The Bitterroot Mountains in southwestern Montana represent a unique landscape where formerly glaciated north-facing slopes are juxtaposed with south-facing slopes whose dominant erosive processes are fluvial bedrock incision and mass wasting. Twelve east-west trending canyons are chosen in this area with Bass Creek Canyon the northernmost and Rock Creek Canyon the southernmost. High-resolution digital elevation models (DEMs) are used to quantify both south- and north-facing slopes to better understand glacial influences on landscape evolution. Hypsometry, sub-ridgeline relief, slope angles, and tributary longitudinal profiles are derived from 10-meter DEMs. Average south-facing slope angles are much steeper than north-facing slopes ( $34^\circ$  compared to  $28^\circ$ ) and hypsometric analyses suggest that north-facing slopes have experienced enhanced erosion with a greater area represented at lower elevations. Geophysical relief calculations also show that a significantly greater volume of material has been glacially eroded on north-facing slopes. Glacial denudation also varies up-canyon to the west. The upper reaches of longitudinal stream profiles show more concave forms up-canyon above paleo-equilibrium line altitudes (ELAs). This study demonstrates that glaciers have effectively moved ridgelines at a faster rate than fluvial and other nonglacial processes. Glaciated cirque basins represent an important hydrologic unit both in terms of snow accumulation and delayed snow-melt as snowfields persisting into summer months provide a significant source of summer streamflow. Therefore, improving our understanding of alpine landscape evolution is essential to managing water resources.

## ACKNOWLEDGEMENTS

First of all, I would like to thank my wonderful fiancée Jenny Baize who has been a great source of encouragement and patience during my research and graduate school experience. My parents, Jon and Sandra Naylor, have also provided a tremendous amount of support during this endeavor and have been fabulous in fostering my education from the beginning. I also thank my advisor Manny Gabet for sharing his bountiful knowledge of geomorphology and GIS as well as providing the initial inspiration for the research. Brian Collins also provided vital assistance in times of GIS turmoil. Dick Gibson and Ryan Portner assisted me with my reconnaissance field work in the Bitterroots and for that I am also obliged. The research was partly funded by a Higher Education Scholarship from the Montana Association of Geographic Information Professionals (MAGIP). The AML code for extracting longitudinal profiles was written by Nathan Niemi while Eric Kirby wrote the Matlab code for obtaining max, min, and mean elevations across a swath. I would also like to thank David Tarboton of Utah State University for providing important dialogue regarding sublimation from alpine snowpacks, as well as Joel Harper for providing a great source of information regarding glacial processes. Ulrich Kamp also provided valuable information regarding the analysis of glaciated terrains and Donald Hyndman provided his expertise regarding the structure and lithology of the Bitterroot Core Complex.

## TABLE OF CONTENTS

Title Page.....	i
Acknowledgements.....	ii
Abstract.....	iii
Table of Contents.....	iv
List of Figures.....	vi
List of Tables.....	vii
List of Plates.....	viii
Introduction.....	1
Study Area.....	4
<i>Geomorphology</i> .....	5
Trunk Streams.....	5
South-facing Slopes and Tributary Drainages.....	6
North-facing Slopes and Tributary Drainages.....	7
<i>Glacial History</i> .....	8
<i>Bedrock Lithology</i> .....	10
<i>Bitterroot Valley Sediments</i> .....	11
Regional Climate Patterns.....	12
<i>Paleo-climate Simulations</i> .....	12
<i>Current Weather and Climate</i> .....	13
<i>Precipitation Gradients</i> .....	14
Methods.....	15
<i>Data</i> .....	15
<i>Watershed Delineation and Division</i> .....	15
<i>Modeling the Upper Extent of Valley Glaciers</i> .....	16
<i>Slope Calculations</i> .....	17
<i>Canyon Asymmetry</i> .....	18
<i>Geophysical Relief</i> .....	18
<i>Hypsometric Analysis</i> .....	19
<i>Longitudinal Profiles</i> .....	20
Results.....	20
<i>Modeled Ice Surfaces</i> .....	20
<i>Slope Calculations</i> .....	21
<i>Relief Calculations</i> .....	21
<i>Asymmetry</i> .....	22
<i>Hypsometric Analysis</i> .....	22
<i>Longitudinal Profiles</i> .....	22
Discussion.....	23

Conclusion.....	31
References.....	32
Appendix: DEM Metadata.....	57

## List of Figures

Figure 1. Map of the central Bitterroot Mountains.....	37
Figure 2. Cross-sectional profile along Blodgett and Mill Creek Canyons.....	38
Figure 3. Geomorphic Features in Blodgett Canyon.....	39
Figure 4. Fred Burr Canyon Valley Cross-section 2.2 km Up-canyon.....	40
Figure 5. Fred Burr Canyon Valley Cross-section 12.0 km Up-canyon.....	40
Figure 6. Interfluves Used to Interpolate Pre-erosional Surface, Kootenai.....	41
Creek Canyon	
Figure 7. Spline Surface Interpolated through Interfluves, Kootenai.....	41
Creek Canyon	
Figure 8. Orthophoto File Overlain on a DEM Showing Approximate.....	42
Location of Trimline, Fred Burr Canyon	
Figure 9. Orthophoto File Overlain on a DEM Showing Modeled Ice.....	42
Surface, Fred Burr Canyon	
Figure 10. Blodgett Canyon South-facing Slope Histogram.....	43
Figure 11. Blodgett Canyon North-facing Slope Histogram.....	43
Figure 12. Geophysical Relief vs. Mean Elevation.....	44
Figure 13. Asymmetry vs. Mean Elevation.....	44
Figure 14a. Bass Creek Canyon Hypsometry.....	45
Figure 14b. Kootenai Creek Canyon Hypsometry.....	45
Figure 14c. Big Creek Canyon Hypsometry.....	45
Figure 14d. Fred Burr Canyon Hypsometry.....	45
Figure 14e. Mill Creek Canyon Hypsometry.....	46
Figure 14f. Blodgett Canyon Hypsometry.....	46
Figure 14g. Canyon Creek Canyon Hypsometry.....	46
Figure 14h. Roaring Lion – Sawtooth Canyon Hypsometry.....	46
Figure 14i. Lost Horse Canyon Hypsometry.....	47
Figure 14j. South Lost Horse Canyon Hypsometry.....	47
Figure 14k. Rock Creek Canyon Hypsometry.....	47
Figure 15. Kootenai Creek Canyon Stream Profile Locations.....	48
Figure 16. Kootenai Creek Canyon Longitudinal Profile Comparison.....	48
Figure 17. Blodgett Canyon Stream Profile Location.....	49
Figure 18. Blodgett Canyon Longitudinal Profile Locations.....	49
Figure 19. Diagram Displaying the Effects of Main Valley Glaciation.....	50
on Tributary Fluvial Basins	

## **List of Tables**

Table 1. Summary of Shear Stress Calculations.....	51
Table 2. Slope Analysis Results.....	51
Table 3. Geophysical Relief Results.....	52
Table 4. Asymmetry and Hypsometry Results.....	52

## List of Plates

Plate 1. Geology of the Central Bitterroot Mountains.....	(in pocket)
Plate 2. Sleeping Child Canyon.....	53
Plate 3. Bedrock Reach along Blodgett Creek.....	53
Plate 4. Step-pool Reach along Kootenai Creek.....	54
Plate 5. Cascading Reach along Blodgett Creek.....	54
Plate 6. Pool-riffle Reach along Bass Creek.....	55
Plate 7. North-south Trending Fractures in Sweathouse Canyon.....	55
Plate 8. Truncated Spur in Bass Creek Canyon.....	56
Plate 9. North- and South-facing Slopes Used for Hypsometry, Slope,.....	(in pocket)
Relief, and Asymmetry Analyses	



## **Introduction**

Mean elevations along the west coast of North and South America are spatially coincident with paleo equilibrium line altitudes (ELAs) (Broecker and Denton, 1990) suggesting that once mountains are uplifted past ELAs (or ELAs are lowered due to climate change) glaciers form and quickly lower the terrain. The pattern implies that glacial erosion exceeds non-glacial erosion as supported by Anderson (2005) who notes that mechanical erosion is typically an order of magnitude greater in glacial catchments and by Hallet et al. (1996) who found that sediment yields increase with glacial ice cover in Alaska.

Several researchers have attempted to compare the effects of glacial and fluvial erosion on landscapes (e.g. Brocklehurst and Whipple, 2005; Kirkbride and Matthews, 1996; Montgomery, 2002). Montgomery (2002) used valley cross-sections from basins glaciated to varying degrees in the Olympic Mountains of western Washington to support the hypothesis of increased erosion due to glacial processes. He found that relief increases as one moves down-valley for both fluvially and glacially carved watersheds, but that glaciated terrain tends to show far greater relief enhancement. However, a fundamental problem with the study is that fluvial and glacial processes have both left prominent signatures on the observed landscape; therefore, the amount of relief production solely attributed to glacial processes is difficult to constrain. Brocklehurst and Whipple (2002) determined that relief enhancement by glaciers is dependent upon basin size, and restricted to topography above the equilibrium line altitude (ELA). Through fluvial and glacial longitudinal profile analysis they (Brocklehurst and Whipple,

2002) concluded that glacial erosion exceeds fluvial erosion only in terms of horizontal headwall incision, a poorly understood process: “further studies of the mechanisms of, and the controls on, headward erosion by alpine glaciers are warranted (Brocklehurst and Whipple 2002).”

The effects of headwall expansion are most profound where east-west trending ridgelines in glaciated and formerly glaciated regions display asymmetric form. G.K. Gilbert (1904) was one of the first to document watershed asymmetry produced by glacially eroded slopes adjacent to non-glaciated slopes in the Sierra Nevada. More recently, Oskin and Burbank (2005) observed ridgeline retreat due to glacial erosion in the Kyrgyz Range of central Asia where uplift and glacial erosion are concurrent. Tuck (1935) also documented asymmetrical drainages within the Kenai Peninsula, the Talkeetna Mountains, and the Chugach Mountains of Alaska. Tuck’s (1935) quantitative analysis was limited to valley cross-sections that indicated southward ridgeline movement of a half mile or more based on the assumption that the drainages were symmetrical prior to glaciation. Tuck (1935) discussed the compounding effects of fractures and sedimentary bedding planes on his research in detail. This difficulty is faced by many researchers comparing glacial and non-glacial erosion as an unbiased study must hold precipitation and lithology constant.

The Bitterroot Front Range represents an ideal region to compare glacial and non-glacial erosion where the main valleys of the range are oriented almost exactly east-west (Figure 1). Beaty (1961) concluded that microclimatic controls (e.g., slope exposure) have worked autonomously in creating the Bitterroots’ asymmetrical watersheds (i.e., in the absence of lithologic and structural controls). North-facing canyon slopes have been

graven by cirque glaciers while south-facing slopes and sub-basins generally lack signs of glacial incision (e.g. circular basin morphometry). Figure 2 displays cross-sectional minimum, maximum, and mean altitudes for a rectangular swath (8 km wide, 12 km long) encompassing Blodgett and Mill Creek Canyons. The line depicting maximum values represents the height of interfluves spanning the watersheds from ridgeline to valley bottom. The maximum elevations along these cross-sections are fairly uniform from one side of the canyon to the other suggesting valley symmetry prior to late Cenozoic glacial incision (Figure 2). Minimum cross-sectional elevations portray the topography of sub-basins and highlight the effects of glacial denudation: a U-shaped trough exists at the bottom of the canyons, north-facing slopes have been flattened due to cirque overdeepening, and overall asymmetry is much greater. East-west trending watersheds in the surrounding area eroded solely by fluvial processes do not demonstrate the observed asymmetry (Plate 2).

Consistent with Beaty's (1961) conclusions, subsequent geologic mapping of bedrock within the region (Lonn and Berg, 1996; Lewis, 1998) shows a massive assemblage of granite with no structural features that might influence intra-basin erosional processes. Weather patterns across the range show a dominant west to east trend (Finklin, 1983) indicating that precipitation is also held constant between north- and south-facing slopes. With precipitation and lithology uniform, the variance in erosional signatures must be attributed to aspect and solar insolation. The effects of aspect on glacial mass balance are poorly understood. Evans (2005) used vector and Fourier analysis on present day glaciers in hopes of gaining a better understanding of historic glacial distributions. Using World Glacier Inventory (WGI) data, he found that aspect

has its greatest influence in mid-latitude regions (30-70 degrees). Contrary to Evan's (2005) findings, several researchers have argued that aspect has little control on cirque development (e.g. Trenhaile, 1976 and Gordon, 1977). Olyphant (1981) proposed that topographic shading has greater controls on radiation reduction than aspect.

Nevertheless, it appears aspect has strongly influenced differential slope erosion for the Bitterroot's main canyons. Therefore, the Bitterroot Front Range represents an ideal study area to observe and quantify the effects of glacial headwall erosion. The prominent asymmetry expressed in the topography of the range is a direct result of ridgeline movement due to glacial denudation.

### **Study Area**

This research encompasses most of the Bitterroot Mountains, a geomorphic province bounded on the west by the Montana – Idaho border and on the east by the Bitterroot Valley. The range represents a prominent east-west drainage divide and extends longitudinally from Lolo Creek in the north to the West Fork of the Bitterroot River in the south. Numerous east-west trending streams flow east from the divide to the front of the range and then over unconsolidated sediments before emptying into the Bitterroot River.

Twelve of these Canyons were chosen for the study ranging from Bass Creek Canyon in the north to South Lost Horse Canyon in the south (Plate 1). Two of the watersheds, Sawtooth Canyon and Roaring Lion Canyon are separated by a low-lying interfluvium, therefore, consistent with a previous study (Beaty, 1961), asymmetry and

other parameters are compared for the north-facing slope of Roaring Lion Canyon and the south-facing slope of Sawtooth Canyon.

## *Geomorphology*

### Trunk Streams

Although most of the streams are ungauged, USGS annual streamflow data exists for Blodgett, Fred Burr, Kootenai, and Rock Creek indicating average streamflows of 2.0, 1.5, 2.3, and 4.3 m<sup>3</sup>/s respectively (<http://nwis.waterdata.usgs.gov/nwis>). The primary unconsolidated sediment within the canyons is glacial till and reworked glacial deposits. This is evident by the general hummocky topography of the till dominated valley bottoms and stream beds that primarily consist of cobbles and boulders.

The trunk streams' upper reaches are fed by headwaters originating from north or northeast facing cirques (e.g. Blodgett, Fred Burr Canyons). Tarn lakes are scattered throughout the headwater regions, some of which have been dammed for irrigation and recreational uses (e.g. Bass Creek Canyon). The upper longitudinal profiles of the channels are characterized by steps typical in glaciated valleys and by overdeepenings formed at tributary junctions (MacGregor et al., 2000). The main streams typically flow over bedrock along these reaches (Plate 3). Other up-stream reaches are typically step-pool reaches (Plate 4), as defined by Montgomery and Buffington (1997), alternating between boulder-filled turbulent runs and finer grained runs with relatively tranquil flow. Woody debris is common throughout the upper reaches and has a strong influence on channel morphology.

The lower reaches of the trunk streams are typically characterized by both step-pool reaches as well as pool-riffle and cascading reaches. Cascading reaches are common near the lower elevations where higher discharges and steep slopes exist, creating tumbling flow over cobbles and boulders (Montgomery and Buffington, 1997). Plate 5 shows a cascading reach of Kootenai Creek while Plate 6 shows a pool-riffle reach along Bass Creek with abundant woody debris present. The trunk streams emerge from canyons cutting through Pleistocene morainal deposits and outwash fans in route to the Bitterroot River.

#### South-facing Slopes and Tributary Drainages

South-facing slopes have primarily been eroded by fluvial bedrock incision, periglacial processes, isolated glacial erosion, and mass wasting processes. Fluvial processes are more evident on south-facing slopes in the three northern canyons cut by Bass Creek, Big Creek, and Kootenai Creek. Most of these streams are ephemeral, cluttered with woody debris, and lacking clearly defined channels. The upper reaches of these channels are most likely dominated by colluvial processes with sediment transported to the centers of sub-basins by soil creep, tree-throw, and burrowing (Montgomery and Buffington, 1997). The southern canyons show signs of mass wasting on south-facing slopes more so than fluvial processes. For example, Blodgett Canyon displays numerous talus slopes along the canyon walls, most likely the result of mass wasting in the form of rock fall or debris flow (Figure 3).

Periglacial processes include nivation, freeze thaw action, and avalanches. Nivation hollows are typically regarded as overdeepened sub-basins showing some

elements of cirque form, but generally lack pronounced features typical of long term erosion due to ice movement (Vilborg, 1977). Solifluction and increased chemical weathering are two processes attributed to the overdeepening of nivation surfaces (Rapp, 1984). Figure 3 displays the location of nivation hollows within Blodgett Canyon.

### North-facing Slopes and Tributary Drainages

As Beaty (1961) noted, north-facing slopes in the Bitterroots bear the signature of prominent glacial erosion. A strong preference for cirque development on north-facing slopes was also noted by Federici and Spagnolo (2004) in the French-Italian Alps where 37% of cirques occurred within the 315-345° (where true north is 0°) aspect interval (this is especially striking considering that only 6% of the slopes in the study were north-facing). King (1974) acknowledged a strong preference for northeast facing cirques in mid- to high- latitudes in the northern hemisphere, primarily due to decreased insolation on north-facing slopes.

Cirque morphology has been extensively studied by several authors (e.g., Federici and Spagnolo, 2004; Olyphant, 1981; and Vilborg, 1977). Most all recognize the semi-circular shape of cirque headwalls in plan view attributed to relatively uniform erosion occurring in horizontal directions. Horizontal cirque growth is driven by frost shattering, pressure release jointing, high transport efficiency, and some amount of abrasion while overdeepening is fostered by abrasion via rotational sliding and alternating expansive and compressive flow (Vilborg, 1977). Identification of cirques is commonly accomplished through topographic map and aerial photo analysis. Rudberg (1954) used the following

classification scheme to describe cirques in the Scandinavian mountains (as outlined by Vilborg, 1977):

*A:1* – Well developed, large glacial cirques with semi-circular form and overdeepened bottoms

*A:2* – As *A:1*, but less developed. No overdeepened bottoms.

*B:1* – Hanging glacial cirques, relatively well developed, but smaller than *A:1*. Their bottoms are often not particularly smooth.

*B:2* – As *B:1*, but less well developed. They seem to originate from fluvial valley ends.

*C:1* – Well developed glacial cirques, forming the ends of trough valleys.

*C:2* – Less developed cirques, forming the ends of trough valleys. Their backwalls are poorly defined or even missing, perhaps because of the relation to rock structure.

*D* – Asymmetric cirque forms, mainly small. Many may be mainly a result of nivation or plucking by the inland ice.

*E* – Rock walls, reminding of cirques because they are slightly concave. Such a wall may be the location for a small wall-sided glacier unless it is formed by nivation only.

Figure 3 shows 6 north-facing cirques in Blodgett Canyon that are identified based on Rudberg's classification scheme. Classification of cirques is somewhat subjective, but it is evident that the cirques show a general increase in size and development in the up-canyon direction.

### *Glacial History*

Alden (1953) produced the first detailed study of glaciation in the Bitterroots. He used moraine morphology to infer relative ages of glacial deposits at the mouths of several canyons ranging from Carlton Creek in the north to Tin Cup Creek in the south. He concluded that the Bitterroots experienced three major glaciations correlating to Early



Pleistocene, Illinoian (or Early Wisconsin), and Wisconsin ages. These were also compared with Richmond's (1965) Pinedale, Bull Lake, and Pre-Bull Lake sequences respectively.

Weber (1972) used granite-weathering ratios, topographic position, and soil development to establish relative dates for glacial deposits along the Bitterroot Front and correlated the deposits with Glacial Lake Missoula lake stands. Consistent with Alden's findings, three main drift sequences were mapped with each sequence overlain by an interglacial paleosol: Judd Drift (probable pre-Wisconsin), Charlos Drift (probable early Wisconsin), and Lost Horse Drift (probable late Wisconsin). The latter includes three main members, but there is evidence of more glacial advances as Weber (1972) mapped 6 end moraines composed of Lost Horse Drift beyond the mouth of Roaring Lion Canyon. He also noted that evidence of glaciation increased as he moved south along the Bitterroot front. Four northern canyons: Carlton, One Horse, Bass, and Kootenai were found to lack the typical U-shape and end moraine complexes at their canyon mouths (Weber 1972). A detailed study of glacial sequences was performed by Weber (1972) on four canyons to the south: Bear, Roaring Lion, Lost Horse, and Rock Creeks. Judd Drift mapped between Lost Horse and Rock Creek Canyons indicate the glaciers from both canyons merged beyond the canyon mouths (Weber 1972). This observation along with the presence of Judd Drift beyond that of other sequences was evidence that Judd (Pre-Bull Lake) aged glaciations were more extensive (Weber 1972).

The distribution of morainal deposits also varies where they extend beyond the mountain front. Weber's (1972) mapped moraines at the mouths of Roaring Lion and Bear Creek Canyons show that the arcuate features are deposited primarily on the south

side of the canyon mouth. Reconnaissance field work for the present study at Fred Burr and Mill Creek Canyons revealed the same distribution of morainal deposits as trunk streams are now forced to flow north around the deposits as they exit into the Bitterroot Valley. The tendency for moraines to be located along the south edge of canyon mouths is further evidence that glacial erosion favored north-facing slopes.

### *Bedrock Lithology*

The Bitterroot Mountains are a metamorphic core complex consisting of metasedimentary rocks in the north and granitic rocks to the south (Lewis, 1998). Intrusive rocks of the Idaho-Bitterroot batholith are Late Cretaceous and Tertiary in age with the eastern plutons displaying crystallization dates between 57 and 53 Ma (Foster and Fanning 1997). Exhumation of the core complex occurred during the Eocene as the region shifted from crustal thickening to extension. The Sapphire Mountains, comprised of Proterozoic Belt Supergroup rocks, moved eastward into western Montana along a detachment fault that left a distinct zone of mylonite along the eastern flank of the Bitterroots (Foster et al. 2001). Fission track dating along the lower easternmost portions of the Bitterroot Front suggests that the mylonite was exposed by Early Miocene time (Foster and Raza, 2002). The mylonite zone is prominent along the lower reaches of each canyon. Mylonite transitions into Belt metasedimentary rocks in Bass, Big, and Kootenai Canyons as one moves up-canyon and into granitic rocks in canyons to the south (Plate 1). There is no lithologic variation between north-facing and south-facing slopes.

The drainage patterns within the Bitterroots are strikingly regular. The east-west trend of the main canyons is most likely attributed to the east-sloping nature of the Bitterroot Dome (Hyndman, personal communication) and the base level control imposed by the Bitterroot Valley to the east. Beaty (1961) postulated that the prominent north-south trend of tributary drainages is controlled by bedrock fractures. Such north-south trending fractures are visible within the mylonite zone (Plate 6) and are most likely the result of brittle response to eastward directed tectonic unloading (Hyndman, personal communication), however, there are no signs of east-west trending structural features that might influence basin asymmetry as outlined by Keller (1996).

Lifton (2005), used a Schmidt Hammer to study rock strength in the Salmon River Mountains to the southwest. He found that for varying lithologies, south-facing slopes consistently showed lower rebound data when compared to north-facing slopes. He concluded that two processes contribute to this phenomenon: 1) increased diurnal fluctuations in temperature exist on south-facing slopes thereby creating temperature gradients whose resulting stresses lead to fracturing and 2) south-facing slopes experience a greater number of freeze-thaw cycles during the winter that favor joint propagation and growth. It is assumed that rocks in the Bitterroot behave similarly and that south-facing slopes most likely exhibit “weaker” rocks due to these processes.

### *Bitterroot Valley Sediments*

Bitterroot Valley sediments contain a geologic record that can be correlated to the evolution of the Bitterroot Range’s landscape. Each of the studied canyons flows into the valley to the east, which establishes base level control at the canyon mouths. A detailed

chronology of normal faulting is lacking, but as noted, Foster and Raza (2002) give an early Miocene date for the exposure of low lying mylonite. Lonn and Sears(1998) generated the most recent and extensive geologic map of the valley, which shows that Quaternary surficial deposits in the form of glacial till and alluvium are more widespread along the Bitterroot Front while Tertiary alluvial deposits predominate along the eastern valley margins. Streams are now incising through morainal deposits and Pleistocene alluvial fan deposits which form terraces along the Bitterroot front. Weber (1972) mapped three main terrace sequences: 1) the Dutch Hill terrace (pre-Bull Lake, possibly associated with the Judd Drift), 2) the Hamilton terrace (Bull Lake age associated with the Charlos Drift), and 3) the Riverside terrace (Pinedale age associated with the Lost Horse Drift). McMurtrey et al. (1959) suggest Pleistocene deposits up to 100 feet in thickness. Tertiary deposits reach thicknesses of 2,400 feet and include both ancestral Bitterroot River deposits and sediments of the Sixmile Creek Formation (McMurtrey et al., 1959).

## **Regional Climate Patterns**

### *Paleo-climate Simulations*

Pleistocene paleo-ELA reconstructions show that alpine glaciers in the Bitterroot Mountains moved significantly further down-valley when compared to other central and western Montana regions (Locke, 1989). The Bitterroot Mountains created an efficient orographic barrier to Pacific moisture, whereas most other mountain ranges in Western Montana were generally lacking a persistent source of precipitation (Locke, 1989).

During Pinedale maxima (~18,000 years ago), summer temperatures were as much as 10°

C cooler than the present and precipitation was reduced due to a southerly shift in the jet stream (Thompson et al., 1993). Kutzbach et al. (1993) suggest the presence of an anticyclonic cell created by the ice sheets that could have imposed easterly winds over the northwestern United States.

### *Current Weather and Climate*

A recent comprehensive study of weather and climate for the region is not available for the Bitterroot geomorphic province. Finklin (1983) produced the only known publication regarding this topic based on a limited data set that included publications from the former U.S. Weather Bureau and fire-weather observations (from stations operational during July and August). The two primary sources for climate data are SNOTEL sites located north of the study area at Lolo Pass and south of the study area at the Nez Perce Camp.

Finklin (1983) found that high altitude wind patterns for the Bitterroot-Selway Wilderness generally follow the prevailing westerlies. Ranger station data at lower elevations on the east side of the divide show a 68% frequency from the west or southwest, a product of down-canyon winds. Free atmosphere conditions display wind directions from the west and typically from the northwest in winter months (Finklin, 1983). He also notes the existence of daytime up-canyon winds on south-facing slopes. However, this observation was most likely made during the summer months when this effect is most noticeable (fire season data). These up-canyon winds are most likely limited during winter months due to a lower angle of incidence and changes in albedo.

Therefore, the role up-canyon winds play in re-distributing snow is most likely insignificant.

### *Precipitation Gradients*

Cold air has the ability to hold less moisture when saturated compared to warmer air and, therefore, precipitation generally increases as air moves up. This phenomenon is evident in the Bitterroot Mountains as precipitation increases as one moves east towards the Bitterroot Divide and decreases as one moves westward away from the divide (Finklin, 1983). Finklin's (1983) precipitation data show that a steep east-west gradient exists, but little variation exists from north to south and vice versa. These data are supported by the Parameter-elevation Regressions on Independent Slopes Model (PRISM) which demonstrates a gradual increase in mean annual precipitation from west of the divide and a steep decreasing gradient toward the Bitterroot Valley to the east. This indicates that precipitation on north- and south-facing slopes within canyons should be uniform.

Consistent with Finklin's data (1983), Weber (1972) cited unpublished data that indicated annual precipitation at the Bitterroot front at approximately 76 cm while the Sapphire Mountains to the east received as little as 18 cm per year. He also noted that Bitterroot Valley paleosols contain widespread caliche horizons along the eastern side of the valley but not along the western valley margins. This indicates that a west-east precipitation gradient existed in the Pleistocene.

Stegman (1998) sighted SNOTEL data that indicate a general thinning of the snowpack from north to south and a decrease in temperature. He attributes this thinning

to the presence of northwesterly prevailing storm tracks which deposit most of the Bitterroots annual precipitation in the form of snow (mid winter – early spring). Only two SNOTEL sites were used for these interpretations and the thick snowpack near Lolo Pass could be due to topographic convergence of storm systems through the pass and Lolo Creek Canyon.

## **Methods**

### *Data*

High resolution 10-meter digital elevation models (DEMs) produced by the United States Geological Survey (USGS) were used in the study (metadata included in Appendix A). The data were downloaded as individual quadrangles and merged into two main DEMs in ArcGrid. The Fill command was used in ArcGrid to correct all sinks by setting those cells equal to their lowest surrounding cell that then becomes the cells pour point. Previous research using DEMs to quantify glaciated terrain (e.g. Brocklehurst 2005) used 30-meter data therefore this study includes higher spatial resolution that enhances certain analyses (e.g. longitudinal profiles).

### *Watershed Delineation and Division*

A flow routing routine was used in ArcGrid to extract individual watersheds from the 2 main DEMs. Watershed pour points were selected at the range front unless the targeted drainage network was intersected by another canyon west of the front. Watersheds were then divided into north and south slopes along the main trunk stream, the location of which was derived using a flow routing algorithm in ArcGrid. Some of

the canyons have distinct bends in the upper reaches of their trunk streams (e.g. Fred Burr) so the division was continued along an east-west trending line in these instances.

### *Modeling the Upper Extent of Valley Glaciers*

Each of the canyons contained a valley glacier during the last glacial maxima as noted in previous research and expressed in prominent U-shaped valley cross-sections. Therefore, in order to truly isolate glaciated slopes from non-glaciated slopes, a general model of main valley glaciers was established so that subsequent analyses could be performed above their ice surface.

Multiple valley cross-sections were used to determine trimline elevations on south-facing slopes where they were most easily distinguished. The cross-sections were taken along truncated spurs (Plates 5, 8) and prominent breaks in slope were marked as the upper extent of ice (Figures 4 and 5 display valley cross-sections for Fred Burr Canyon at 2.2 and 12 km up-canyon respectively). Slope breaks were not as discernable on north-facing slopes where hanging tributary valleys make it difficult to establish an ice elevation for the main valley. Ice elevations were taken from south-facing truncated spurs, extrapolated across-canyon to the north-facing slope, and a spline surface (interpolation method that fits a surface between points with minimum curvature) was used to interpolate the points thus creating a “snapshot” model of a paleo-ice surface.

Digital orthophoto files were overlain on DEMs to assist in distinguishing glacial features (e.g. lateral, terminal moraines). Reconnaissance field work was also conducted to check the accuracy of the modeled ice surface. Slopes were often too steep to traverse



and elevations of spurs, slope breaks, or lateral moraines were located on topographic maps in these instances.

Basal shear stress was calculated for each cross-section within each canyon to test the modeled ice elevations. Basal shear stress ( $\tau_b$ ) along the center-line of the modeled glacier is calculated with (Paterson, 1981):

$$\tau_b = F\rho gh \sin \alpha$$

where  $F$  is a shape factor (0.709 for most canyons),  $\rho$  is density (900 kg/m<sup>3</sup>),  $g$  is gravity (9.81 m/s<sup>2</sup>),  $h$  is centerline thickness determined from trimline elevation and valley bottom elevation, and  $\alpha$  is the slope (in degrees) of the ice surface. The shape factor incorporates the influence of valley walls into the shear stress calculation. The value was derived from Paterson's Table 6.1 (1981) for calculated  $W$  values (half valley width divided by depth). The commonly assumed value for mean basal shear stress for glaciers is 1 bar (1x10<sup>5</sup> N/m<sup>2</sup>).

### *Slope Calculations*

Slope histograms were established for north- and south-facing sides of each canyon above the modeled ice surface. The complete north-facing slopes were included in the analysis while some of the up-canyon south-facing slopes were removed due to the presence of cirques (Plate 9). Slopes were calculated in ArcGrid by fitting a plane to a 3x3 grid surrounding the target cell and calculating the slope of the plane in degrees.

### *Canyon Asymmetry*

In order to quantify canyon asymmetry, horizontal distance was measured from valley bottoms to watershed-bounding ridgelines. The horizontal distance from the trunk stream to the southern ridgeline was measured along a north-south trending line, and an average was taken from 10 equidistant measurements. The process was repeated for south-facing slopes but, consistent with the slope analysis, only for the portion of the slopes not distinctly influenced by glaciation. The average north-facing distance was then divided by the average south-facing distance to obtain a N:S ratio.

### *Geophysical Relief*

Measuring relief is difficult due to its somewhat arbitrary nature. DEM analysis resolves this issue by allowing one to easily measure “geophysical relief” as defined by Small and Anderson (1998). This is calculated by dividing the volume of material removed below ridgelines and peaks by the surface area. For this study, geophysical relief is calculated using a modified version of Brocklehurst and Whipple’s (2002) techniques. Their procedure fitted a cubic spline surface between ridgeline points outlining the basin to establish a pre-erosion surface. However, this method introduces significant error due to the underlying assumption that valleys were not incised below ridgelines prior to glaciation. For the present study, a spline surface is fitted between points outlining the basin and points located along tributary interfluves. The interfluves show similar slopes along their axis for both north- and south-facing slopes (Figure 2). Therefore, by integrating interfluve points into the spline interpolation we better isolate

post-glacial relief production. Figure 6 shows the interfluves above which an interpolated pre-erosional surface was derived for Kootenai Canyon (Figure 7). The current topography was subtracted from the surface using the “cut and fill” command in ArcMap yielding the vacated volume of material. In some instances, the upper-canyon south-facing slopes were omitted to avoid the inclusion of glaciated terrain

### *Hypsometric Analysis*

Hypsometric curves depict the proportion of a basin’s area that exists above a given elevation (Ritter et al., 1996). The hypsometric integral (*HI*), the area under the curve, is unique for particular curve shapes and is used as an indicator of basin dissection or stage in landscape evolution. The integral is estimated using the following relationship:

$$HI = \frac{H_{mean} - H_{min}}{H_{max} - H_{min}}$$

where  $H_{mean}$ ,  $H_{max}$ , and  $H_{min}$  are the mean, maximum, and minimum basin elevations (Brocklehurst and Whipple, 2004). The curve’s shape also represents properties of landscape evolution as a convex shape generally represents youthful landscapes while extremely concave curves represent mature landscapes (Strahler, 1952). Hypsometric curves were generated for north-facing and south-facing slopes in each canyon with ArcMap. The influence of varying area from one slope to another is minimized by graphing normalized values.

## *Longitudinal Profiles*

Longitudinal profiles for tributary valleys feeding into the main canyons were extracted from watershed DEMs using an ARC Macro Language (AML) script. A minimum area of  $0.3 \text{ km}^2$  was used to delineate the sub-basins and a minimum flow accumulation of  $0.01 \text{ km}^2$  was used to establish the headwaters of the tributary streams. Various combinations were tested but these values produced the most complete longitudinal profiles without including numerous low order stream channels.

## **Results**

### *Modeled Ice Surfaces*

Figure 8 displays an orthophoto file overlain on a DEM of Fred Burr Canyon, and Figure 9 shows the corresponding modeled ice surface. Table 1 contains average ice elevations and average calculated shear stresses for each canyon. Most glaciers have basal shear stress values between  $5 \times 10^4 \text{ N/m}^2$  and  $1.5 \times 10^5 \text{ N/m}^2$  (Paterson, 1981); with the exception of Kootenai Creek each of the canyon ice models are within this range suggesting that the estimated ice surfaces are reasonable. The terminus of the Kootenai Canyon glacier existed at approximately 1200 meters near the high stand of Glacial Lake Missoula during the Lost Horse Drift glacial maxima so calving might explain this anomalously high shear stress value. The terminus ice elevation was assumed to be at ground level for the shear stress calculation, but it may have been higher due to the calving of the glacier.

### *Slope Calculations*

Average slopes were calculated for the northern and southern halves of each canyon. Slope aspects vary within sub-basins, therefore the slope results represent composite slope values for the north- and south-facing sides of each canyon. Figures 10 and 11 are histograms displaying the distribution of slope values for the glaciated and non-glaciated terrains in Blodgett Canyon. Slope values for each canyon are summarized in Table 2 along with the standard deviation for each drainage aspect. The average slope for glaciated terrain 27.7 degrees, is lower than the average slope for non-glaciated terrain, 33.7 degrees (t-test,  $P < 0.001$ ). Standard deviation also varies with aspect and glacial influence as north-facing and south-facing slope analyses produced standard deviations of 11.9 and 9.6 degrees respectively (t-test,  $P < 0.001$ ).

### *Relief Calculations*

Geophysical relief values are listed in Table 3. North-facing slopes demonstrate greater relief production in each case and several canyons (Fred Burr, Mill Creek, Blodgett, Canyon Creek, and Sawtooth-Roaring Lion) have experienced a nearly two-fold increase in relief production on north-facing slopes. Average north-facing geophysical relief values (221 m) are much greater than those of south-facing slopes (139 m,  $P < 0.001$ ). Standard deviation is 57 m for relief calculations from both slopes. Figure 12 demonstrates the relationship between differential relief production (expressed as a N:S facing relief ratio) and mean watershed elevation.

### *Asymmetry*

The average N:S canyon asymmetry ratio is 1.55 (values are presented in Table 4). These data were compared with other variables (e.g. slope, relief) to determine whether general trends between them and ridgeline movement exist. There is a modest correlation ( $R^2=0.35$ ,  $P<0.001$ ) between asymmetry and mean watershed elevation (Figure 13).

### *Hypsometry*

Average hypsometric integrals are 0.538 for north-facing slopes and 0.561 for south-facing slopes (Table 4, Figures 14a-k). The data are normalized so that the effect of varying analyzed areas is minimized.

### *Longitudinal Profiles*

Longitudinal profiles were extracted and analyzed for all canyons in the study area. Representative drainages are Kootenai Creek Canyon (Figures 25, 26) in the northern part of the study area and Blodgett Canyon to the south (Figures 27, 28). Tributary profiles were chosen at similar distances up-canyon for comparison between aspects.

South-facing tributary profiles along Kootenai Creek Canyon are relatively straight at lower altitudes and increase in concavity as one moves up-canyon (Figure 26). A comparison between profiles 9 (south-facing) and 10 (north-facing) demonstrates that north-facing slopes within the drainage are more concave as altitude increases. Tributary profiles for Blodgett Canyon are straight in the lower reaches of the canyon with very

low concavity, but as one moves up-canyon north-facing profiles show increased concavity in the upper reaches where cirque enlargement is most prominent. This effect is enhanced in profiles further up-canyon, reflecting increased cirque development above the ELA.

## **Discussion**

The modeled ice surfaces represent general reconstructions of the main valley glaciers. It is not suggested that these models are entirely correct as their purpose is to simply remove the glacial trough from the analysis so that glacial and non-glacial processes can be compared. Potential errors in the modeled ice surfaces may be due to incorrect interpretations of cross-valley profiles (e.g. multiple slope breaks) and incorrect interpretations of trimline elevations from aerial photos. Actual error values are impossible to derive, but it is estimated that the ice surfaces lie within 50 meters of the actual ice surface during Pinedale aged glaciations. Furthermore, the modeled ice surfaces represent a “snapshot” in time whereas the extent of glaciers varied through time as they advanced down-valley and retreated during inter-glacials. Previously mapped glacial deposits support the models as the ice surface for Rock Creek Canyon joins lateral moraines near Lake Como at approximately 1585 meters. Weber (1972) mapped the moraines’ till as Lost Horse Drift (correlated to Pinedale age glacial maxima).

Moisture availability is the fundamental component of both glacial and fluvial erosion. Therefore, in order to isolate varying erosional processes as the cause of differential erosion in the Bitterroots, it must hold true that total moisture balances are relatively equal for both north- and south-facing slopes. There are two primary factors

that could lead to moisture differences with respect to aspect: 1) redistribution of snow favoring north-facing slopes, and 2) increased rates of sublimation that lower the amount of water available for erosional processes.

Stegman's (1998) research indicates that avalanche chutes show a strong preference for south-facing slopes, and a lesser, but frequent distribution on northwest facing slopes. Steeper slopes could result in greater avalanche frequency but prior to the onset of glacial maxima, slope angles were most likely comparable for both north- and south-facing slopes making differential distribution of snow unlikely (the occurrence of snow prior to the late Pliocene and Pleistocene is debatable). Currently, snow redistribution away from sub-basins into the main valley is probably greater for the south-facing aspect. However, this is a product of glacial erosion as allometric cirque growth and flattening of cirque bottoms allow cirque laden slopes to retain snow more efficiently (Olyphant, 1981).

Winds are currently dominated by westerlies with a southwest component and no data exist that indicate paleo-wind patterns were different. Erickson et al. (2005) found that wind sheltering is the primary component controlling the spatial distribution of snow in an alpine setting. Each of the tributary canyons show a north-south orientation indicating that the existence of north-south trending interflaves should in theory provide an equal amount of wind sheltering for both north- and south-facing slopes.

Several researchers have studied snowpack sublimation, but little information exists quantifying the influence of aspect on sublimation (Tarboton, written communication). Recent research quantifying sublimation has collected data over an annual cycle as the greatest latent heat fluxes occur during the accumulation season



(Hood et al., 1999). Hood et al. (1999) found that sublimation accounted for 15% of the total snowpack along the Niwot Ridge in Colorado and 13% of annual precipitation for 1994-1995 snow season. They also studied the impacts of wind speed, temperature, specific humidity, and net radiation on sublimation and concluded that wind speed and temperature are the primary influences. In the Bitterroots, wind speed variation on juxtaposed slopes is highly unlikely while temperature variation could cause differential sublimation rates. However, since we lack snowpack data for differing slope aspects, it remains difficult to quantify the amount of temperature induced sublimation within the range. Hood's (1999) research took place on a flat saddle along Niwot Ridge where both high wind speeds and direct insolation are likely to result in sublimation rates exceeding those on any slope in the Bitterroot Range. Although sublimation rates were most likely constant along the Bitterroot Front, snow accumulation or ablation seems to vary longitudinally as suggested by mountain front glacial deposits and asymmetry results.

The three canyons to the north show less asymmetry when compared to other canyons, with the exception of Kootenai Creek Canyon (3:2 N:S stream-ridgeline distance ratio). Varying lithology could influence slope form within the 3 northern canyons where metasedimentary rocks are present (Plate 1). Chase's (1973) geologic map of the petrology and structure of the northeastern Idaho-Bitterroot Batholith displays pelitic schist along Big Creek with a southerly dip to foliation planes, which could create a dip-slope effect for south-facing slopes. As mentioned, the three northern canyons display fewer signs of glacial erosion along their lower reaches when compared to the other canyons (e.g., terminal moraines, U-shaped profile are absent) and the reduced

asymmetry could be a product of limited glacial erosion due to higher paleo-ELAs to the north.

Asymmetry and mean elevation display a slight correlation, which could be more significant ( $R^2 = 0.70$ ) by removing 3 outliers. The outliers for the regression are Bass Creek, Canyon Creek, and Sawtooth-Roaring Lion Canyons. Bass Creek is the northernmost canyon with limited cirque development on its north-facing slope and could justifiably be removed from the analysis, while Canyon Creek is a relatively small drainage that exists at high altitude between Blodgett and Sawtooth Canyons (Plate 9). The fact that Roaring Lion and Sawtooth Canyons are separated by a low interfluvium make it difficult to compare their results as well since mean watershed elevation is calculated from two separate watersheds. The difference in relief production between slopes also increases with elevation as shown in Figure 12. Unlike asymmetry and relief, hypsometry results showed no correlation with mean watershed elevation.

Several authors argue that basin area strongly influences the general shape of hypsometric curves as smaller basins show a more convex curve whereas larger basins demonstrate a more concave, s-shaped curve (e.g. Hurtrez et al. 1999, Sinha-Roy 2002). However, this analysis examines hypsometry variations within basins, but the size of tributary sub-basins does vary. Sinha-Roy (2002) argues that smaller basins tend to be dominated by diffusive processes while larger basins tend to have more extensive channel networks that distribute a greater area to lower elevations. Figures 14a-k demonstrate this general trend for the Bitterroot canyons, but dendritic channel networks are generally lacking on north-facing slopes. Instead, the redistribution of basin area to lower elevations is most likely the product of glacial erosion during the Pleistocene.

Hypsometric integrals (Table 4) are greater for north-facing slopes in 6 of the canyons, consistent with Brocklehurst and Whipples' (2004) findings in the Sierra Nevada and Sangre de Cristo Ranges. The 5 remaining canyons demonstrate greater hypsometric integrals for non-glaciated south-facing slopes consistent with previous findings in the Ben Ohau Range in New Zealand. Brocklehurst and Whipple (2004) attributed this to relative positions of the mean Quaternary ELA ( $ELA_{mean}$ ) for each range as a slight lowering in this parameter can have significant impacts on watershed hypsometry. Weber (1972) as well as Lonn and Sears (1998) show more extensive terminal and lateral moraine deposits along the southern Bitterroot Front signifying a general lowering of the  $ELA_{mean}$  for the southern canyons. Each of the canyons with lower north-facing hypsometric integrals lies to the south and contains a prominent terminal or lateral moraine complex extending beyond the range front suggesting that Brocklehurst and Whipples' (2004) findings hold true for the Bitterroot Range. This effect was originally suggested for fluvial catchments by Strahler (1964) who proposed that a lowering of the hypsometric curve and therefore the hypsometric integral indicates a shift towards landscapes that have been subjected to greater amounts of erosion.

Slope calculations (Table 2) also suggest that glaciers erode more efficiently since north-facing slope values are 6 degrees less than those for non-glaciated areas. Standard deviation values are also greater for glaciated terrain (11.9 versus 9.6 for non-glaciated,  $P < 0.001$ ) indicating that variability is greater on north-facing slopes. The increased standard deviation is most likely caused by the development of steep cirque headwalls adjacent to flat, over-deepened cirque floors.

Slope results for south-facing slopes indicate that the steep nature of these terrains currently support mass wasting processes as opposed to hydraulic activity. As mentioned, Stegman (1998) found that avalanche chutes show preference for south-facing slopes, but previous research has shown that avalanches can represent a minor component of sediment redistribution in alpine terrain (e.g. Gardner, 1986; Caine, 1986). Transport in the form of rock falls and debris flows most likely dominate Holocene sediment transport while transport through bedrock channels (Gardner, 1986) most likely represents a minor component. Numerous coarse-grained talus piles along the base of the south-facing slopes are strong evidence for the erosional importance of mass failures.

Glacial maxima represent major thresholds for alpine catchments through which previously established sub-basins are permanently altered. Brocklehurst and Whipple (2005) and Montgomery (2002) note that valley widening is greater than deepening where valley glaciers once existed. Montgomery (2002) found that glaciated valleys of the Olympic Peninsula expanded at the expense of tributary valleys. This effect is apparent on the south-facing slopes of the Bitterroot canyons where main valley glaciers have cannibalized the lower reaches of tributary drainages that developed during the Tertiary. The effect of widening the main valley walls is outlined in Figure 29. By establishing fluvial hanging valleys, a knickpoint is created along the original channel and disequilibrium follows as the knickpoint migrates up-slope. South-facing longitudinal profiles (Figures 26 and 28) are straight suggesting that the knickpoints have completed their upward migration. By steepening adjacent non-glaciated terrain, glacial erosion may enhance post-glacial sediment transport and continue their legacy of increasing erosion rates. It should be noted as a counter argument that Lifton (2005)

observed oversteepening along the south-facing wall of Big Creek Valley (central Idaho) and attributed it to preferential lateral stream migration towards weaker bedrock.

Therefore, the effect has been observed in fluvial valleys but it seems to be augmented by glacial erosion in the Bitterroots.

Tributary longitudinal profiles demonstrate similar form for each slope at lower elevations near the mouth of each canyon. However, the channel profiles evolve differentially as one moves up-canyon, above paleo ELAs. These results are consistent with Brocklehurst and Whipples' (2002) findings that demonstrate greater headwall retreat above paleo-ELAs. They (Brocklehurst and Whipple, 2002) also point out that glacial erosion exceeds fluvial erosion primarily through headwall retreat. A prominent variation can be seen when comparing headwall retreat between the Bitterroot's north- and south-facing slopes since the upper reaches of north-facing longitudinal profiles have expanded further laterally away from the canyon's trunk streams (Figures 26 and 28). These results are consistent with Brocklehurst and Whipple's (2002) analysis of glaciated longitudinal profiles. They found that glacial erosion is concentrated above paleo-ELAs for smaller basins (similar to the north-facing sub-basins in this study).

Glacial denudation via headwall retreat is only partially described by extracting current longitudinal profiles. The circular form of cirque headwalls is produced by their allometric growth (i.e. they expand in length and width at the same rate). Therefore, in order to understand a glacier's ability to enhance relief, one must consider the three-dimensionality of their collective processes (i.e. headwall sapping). Geophysical relief calculations show that Pleistocene glaciations removed a much greater volume of bedrock when compared to erosional processes that acted upon the terrain prior to glacial

maxima. Glaciated slopes display a near doubling of relief production (Table 3), but this is a conservative estimate of the overall effects on the range since relief production in the main valley is not considered. Although it cannot be concluded that main valleys were significantly deepened, truncated spurs indicate that valley widening did occur (Figures 4, 5). Since the onset of cooler climate approximately 2.4 mya (Ruddiman et al., 1988) glaciers have catalyzed relief enhancement in the Bitterroots and shifted ridgelines to the south. South-facing slopes indicate that fluvial and mass wasting processes that dominated alpine relief production prior to Late Pliocene-Pleistocene glacial maxima were not nearly as efficient.

Several researchers acknowledge that mechanical weathering rates in glacial systems can exceed fluvial rates by an order of magnitude (Anderson, 2005; Hallet, 1996). The number and capabilities of glacial erosional processes is not trivial as abrasion, plucking, pressure release jointing, and basal meltwater all work in concert to enhance denudation (Martini et al., 2001). Recent studies demonstrate that chemical weathering may be greatly enhanced as well (Anderson, 2005). The mechanical processes that break down material increase the surface area subject to chemical attack and thereby enhance chemical weathering. Hence, both mechanical and chemical processes are amplified by the presence of glaciers.

The implications of this research go beyond reconstructing the denudational history of a mountain range. Although the pre-glacial water budget was most likely comparable between north- and south-facing slopes in the Bitterroots, current conditions are quite the contrary. Temporal and spatial snowpack variations have not been studied for any of the Bitterroot watersheds, but it seems intuitive that snowfields would persist

longer into summer months within north-facing cirque basins. Meltwater from these snowfields supports stream baseflow during late summer months when precipitation inputs are minimal. Therefore, understanding how relief structure influences snowpack variations and snowmelt timing could greatly enhance hydrologic models for the Bitterroot Valley where water demands are increasing. The methods presented herein improve our understanding of relief distribution within the Bitterroots, but future work should be focused toward modeling spatial and temporal variations of snowpack within the range.

### **Conclusion**

Glacial erosion has exceeded other denudational processes in sculpting the Bitterroot geomorphic province. By comparing glaciated and non-glaciated terrain, it is demonstrated that relief production is far greater in glacial systems and that a prominent shift in elevation distribution has also occurred. Slope results and longitudinal profiles indicate that glacial maxima represent a profound shift away from pre-glacial equilibrium as south-facing paleo-fluvial networks have been drastically altered. Although the role of sediment transport remains dependent upon fluvial networks beyond glacial termini, the results indicate that glacial erosion dominates alpine landscape evolution where conditions favor the existence of glaciers.

## References

- Alden, W. C., 1953, Physiography and glacial geology of Western Montana and adjacent areas, U.S. Geological Survey Professional Paper, p. 200.
- Anderson, S. P., 2005, Glaciers show direct linkage between erosion rate and chemical weathering fluxes: *Geomorphology*, v. 67, p. 147-157.
- Beaty, C. B., 1961, Asymmetry of stream patterns and topography in the Bitterroot Range, Montana: *Journal of Geology*, v. 70, p. 347-354.
- Brocklehurst, S. H., and Whipple, K., X., 2002, Glacial erosion and relief production in the eastern Sierra Nevada, California: *Geomorphology*, v. 42, p. 1-24.
- Brocklehurst, S. H., and Whipple, K., X., 2004, Hypsometry of glaciated landscapes: *Earth Surface Processes and Landforms*, v. 29, p. 907-926.
- Brocklehurst, S. H., and Whipple, K., X., 2005, Assessing the relative efficiency of fluvial and glacial erosion through simulation of fluvial landscapes: *Geomorphology*, v. Publication pending.
- Broeker, W. S., and Denton, G. H., 1990, What drives glacial cycles?: *Scientific American*, v. 262, p. 48-56.
- Caine, T. N., 1986, Sediment movement and storage on alpine slopes in the Colorado Rocky Mountains, in Abrahams, A. D., editor, *Hillslope Processes*: Boston, MA, Allen and Unwin, p. 115-137.
- Chase, R. B., 1973, Petrology of the northeastern border zone of the Idaho Batholith, Bitterroot Range, Montana, *Montana Bureau of Mines and Geology Memoir #43*, p. 28.
- Erickson, T. A., and Williams, M. W., 2005, Persistence of topographic controls on the spatial distribution of snow in rugged mountain terrain, CO, U.S.A: *Water Resources Research*, v. 41, p. 17.
- Evans, I. S., 2006, Local aspect asymmetry of mountain glaciation: a global survey of consistency of favored directions for glacier numbers and altitudes: *Geomorphology*, v. 73, p. 166-184.
- Federici, P. R., and Spagnolo, M., 2004, Morphometric analysis on the size, shape, and areal distribution of glacial cirques in the Maritime Alps (Western French-Italian Alps): *Geografiska Annaler*, v. 86, p. 235-248.
- Finklin, A. I., 1983, *Weather and climate of the Selway-Bitterroot Wilderness*: Moscow, Idaho, University Press of Idaho, 144 p.



Foster, D. A., and Fanning, C. M., 1997, Geochronology of the northern Idaho Batholith and the Bitterroot Metamorphic Core Complex: magmatism preceding and contemporaneous with extension: *G.S.A. Bulletin*, v. 109, p. 379-394.

Foster, D. A., Schafer, C., Fanning, C. M., and Hyndman, D. W., 2001, Relationships between crustal partial melting, plutonism, orogeny, and exhumation: Idaho-Bitterroot Batholith: *Tectonophysics*, v. 342, p. 313-350.

Foster, D. A., and Raza, A., 2002, Low-temperature thermochronological record of exhumation of the Bitterroot Metamorphic Core Complex, Northern Cordilleran Orogen: *Tectonophysics*, v. 349, p. 23-36.

Gardner, J. S., 1986, Sediment movement in ephemeral streams on mountain slopes, Canadian Rocky Mountains, in Abrahams, A. D., editor, *Hillslope Processes*: Boston, MA, Allen and Unwin, p. 97-113.

Gilbert, G. K., 1904, Systematic asymmetry of crest lines in the high Sierra of California: *Journal of Geology*, v. 12, p. 579-588.

Gordon, J. E., 1977, Morphometry of cirques in the Kintail-Affric-Cannish Area of Northwest Scotland: *Geografiska Annaler*, v. 50A, p. 177-194.

Hallet, B., Hunter, L., and Bogen, J., 1996, Rates of erosion and sediment evacuation by glaciers: A review of field data and their implications: *Global and Planetary Change*, v. 12, p. 213-235.

Hood, E., Williams, M., and Cline, D., 1999, Sublimation from a seasonal snowpack at a continental, mid-latitude site: *Hydrological Processes*, v. 13, p. 1781-1797.

Hurlitz, J. E., Sol, C., and Lucazeau, F., 1999, Effect of drainage area on hypsometry from an analysis of small-scale drainage basins in the Siwalik Hills (Central Nepal): *Earth Surface Processes and Landforms*, v. 24, p. 799-808.

Isard, S. A., 1983, Estimating potential direct insolation to alpine terrain: *Arctic and Alpine Research*, v. 15, p. 77-89.

Keller, E. A., 1996, *Active Tectonics: Earthquakes, Uplift, and Landscape*: Upper Saddle River, N.J., Prentice Hall, 338 p.

King, C. A. M., 1974, Morphometry in glacial geomorphology, in Coates, D. R., editor, *Glacial Geomorphology*: Boston, MA, Allen and Unwin, p. 147-162.

Kirkbride, M., and Matthews, D., 1997, The role of fluvial and glacial erosion in landscape evolution: The Ben Ohau Range, New Zealand: *Earth Surface Processes and Landforms*, v. 22, p. 317-327.

- Kutzbach, J. E., and Ruddiman, W. F., 1993, Model description. external forcing and surface boundary conditions., in Wright, H. E. J. e. a., editor, *Global Climates since the Last Glacial Maximum*: Minneapolis, MN, Univ. of Minnesota Press, p. 12-23.
- Lewis, R. S., 1998, *Geologic Map of the Montana Part of the Missoula West 30' x 60' Quadrangle*, Montana Bureau of Mines Open-File Report #373.
- Lifton, Z. M., 2005, *Bedrock Strength Controls on the Valley Morphometry of Big Creek, Valley and Idaho Counties, Central Idaho*, Geology: Pocatello, ID, Idaho State University, p. 125.
- Locke, W. W., 1989, Present climate and glaciation of Western Montana, U.S.A: *Arctic and Alpine Research*, v. 21, p. 234-244.
- Lonn, J. D., and Berg, R. B., 1996, *Preliminary Geologic Map of the Hamilton 30' x 60' Quadrangle*, Montana Bureau of Mines Open-File Report #340.
- Lonn, J. D., and Sears, J.W., 1998, *Preliminary Geologic Map of the Bitterroot Valley, Montana*, Montana Bureau of Mines Open File Report #362.
- MacGregor, K. R., Anderson, R. S., Anderson, S. P., and Waddington, E. D., 2000, Numerical simulations of glacial-valley longitudinal profile evolution: *Geology*, v. 28, p. 1031-1034.
- Martini, I. P., Brookfield, M. E., and Sadura, S., 2001, *Principles of Glacial Geomorphology and Geology*: Upper Saddle River, NJ, Prentice Hall, 381 p.
- McMurtrey, R. G., Konizeski, R. L., and Stermitz, F., 1959, *Geology and water resources of the Bitterroot Valley*, Montana Bureau of Mines Bulletin, p. 37.
- Montgomery, D. R., and Buffington, J. M., 1997, Channel-reach morphology in mountain drainage basins: *GSA Bulletin*, v. 109, p. 596-611.
- Montgomery, D. R., 2002, Valley formation by fluvial and glacial erosion: *Geology*, v. 30, p. 1047-1050.
- Olyphant, G. A., 1981, Interaction among controls of cirque development: *Sangre De Cristo Mountains, CO, U.S.A: journal of Glaciology*, v. 27, p. 449-458.
- Oskin, M., and Burbank, D. W., 2005, Alpine landscape evolution dominated by cirque retreat: *Geology*, v. 33, p. 933-936.
- Paterson, W. S. B., 1981, *The Physics of Glaciers*, Pergamon Press, 380 p.
- Rapp, A., 1984, Nivation hollows and glacial cirques in Soderasen, Scania, South Sweden: *Geografiska Annaler*, v. 66, p. 11-28.

- Richmond, G. M., 1965, *Glaciation of the Rocky Mountains, The Quaternary of the United States*: Princeton, N.J., Princeton Univ. Press, p. 217-230.
- Ritter, D. F., Kochel, C. R., and Miller, J. R., 2002, *Process Geomorphology*: New York, NY, McGraw Hill.
- Rudberg, S., 1954, *Vasterbottens berggrundsmorfologi*: *Geographica*, v. 25, p. 457.
- Ruddiman, W. F., Raymo, M.E., Lamb, H.H., Andrews, J.T., 1988, Northern hemisphere climate regimes during the past 3 ma: possible tectonic connections [and discussion]: *Philosophical Transactions of the Royal Society of London, Series B, Biological Sciences*, v. 318, p. 411-430.
- Sinha-Roy, S., 2002, Hypsometry and landform evolution: a case study in the Banas Drainage Basin, Rajasthan, with implications for Aravalli Uplift: *Journal Geological Society of India*, v. 60, p. 7-26.
- Small, E. E., and Anderson, R. S., 1998, Pleistocene relief production in Laramide Mountain Ranges, Western United States: *Geology*, v. 26, p. 123-126.
- Stegman, S. V., 1998, Remote Sensing of Avalanche Chutes in the Central Bitterroot Range, Montana, Dept. of Geography, University of Montana, p. 66.
- Strahler, A. N., 1952, Hypsometric (area-altitude) analysis of erosional topography: *G.S.A. Bulletin*, v. 63, p. 1117-1142.
- Strahler, A. N., 1964, Quantitative geomorphology of drainage basins and channel networks, in Chow, V. T., editor, *Handbook of Applied Hydrology*: New York, NY, McGraw Hill, p. 39-76.
- Thompson, R. S., Whitlock, C., Bartlein, P. J., Harrison, S. P., and Spaulding, G. W., 1993, Climatic changes in the Western United States since 18,000 yr B.P., in Wright, H. E. J. e. a., editor, *Global Climates since the Last Glacial Maximum*: Minneapolis, MN, Univ. of Minnesota Press.
- Trenhaile, A. S., 1976, Cirque morphometry in the Canadian Cordillera: *Annals of the Association of American Geographers*, v. 66, p. 451-462.
- Tuck, R., 1935, Asymmetrical topography in high Altitudes resulting from glacial erosion: *Geology*, v. 43, p. 530-538.
- Vilborg, L., 1977, The cirque forms of Swedish Lapland: *Geografiska Annaler*, v. 59, p. 89-150.

Weber, W. M., 1972, Correlation of Pleistocene glaciation in the Bitterroot Range, Montana, with fluctuations of Glacial Lake Missoula, Montana Bureau of Mines and Geology Memoir #42, p. 44.

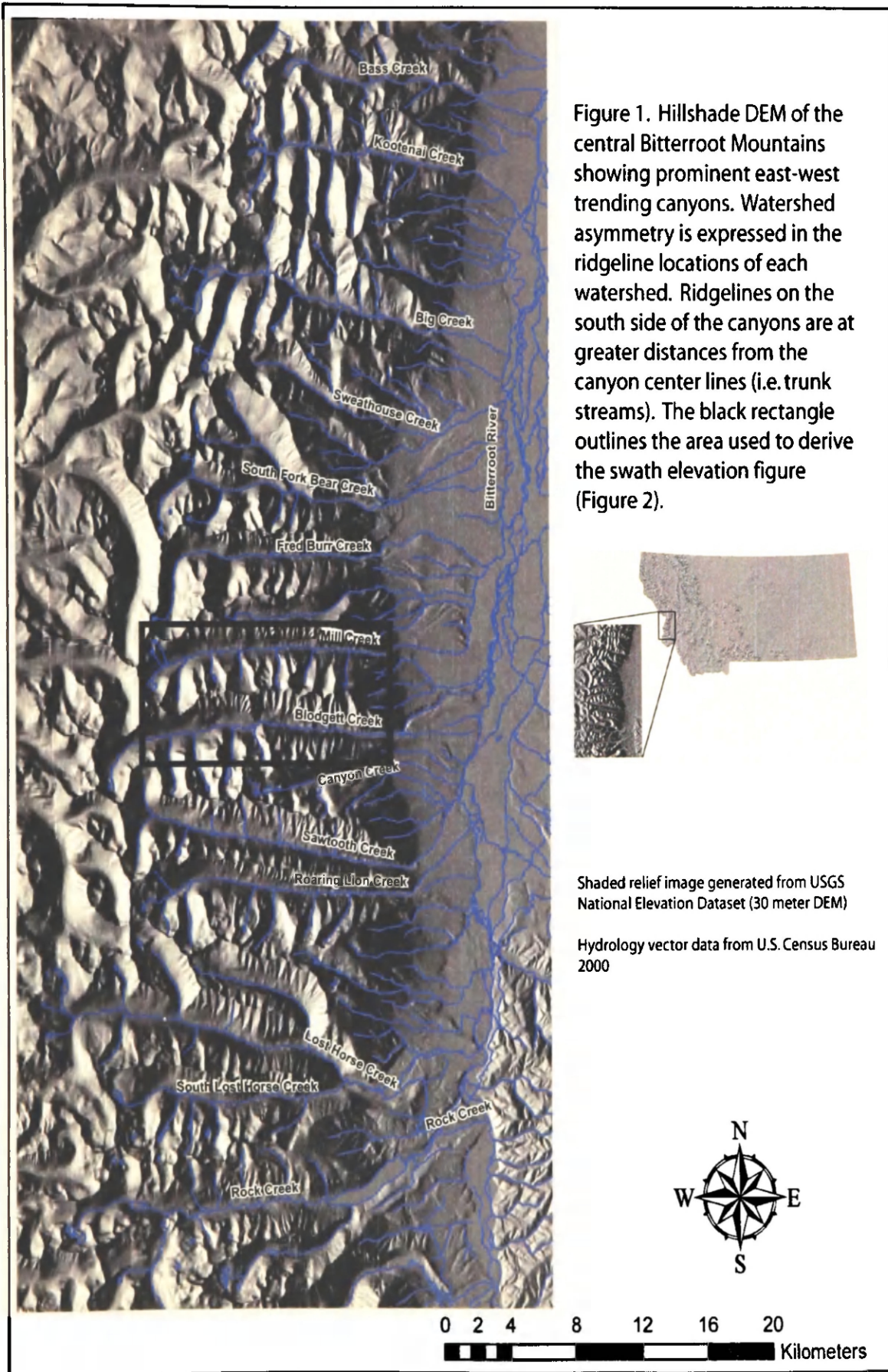
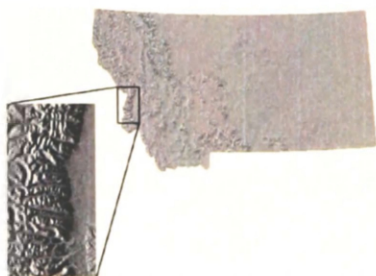
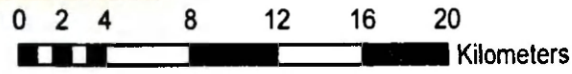


Figure 1. Hillshade DEM of the central Bitterroot Mountains showing prominent east-west trending canyons. Watershed asymmetry is expressed in the ridgeline locations of each watershed. Ridgelines on the south side of the canyons are at greater distances from the canyon center lines (i.e. trunk streams). The black rectangle outlines the area used to derive the swath elevation figure (Figure 2).



Shaded relief image generated from USGS National Elevation Dataset (30 meter DEM)

Hydrology vector data from U.S. Census Bureau 2000



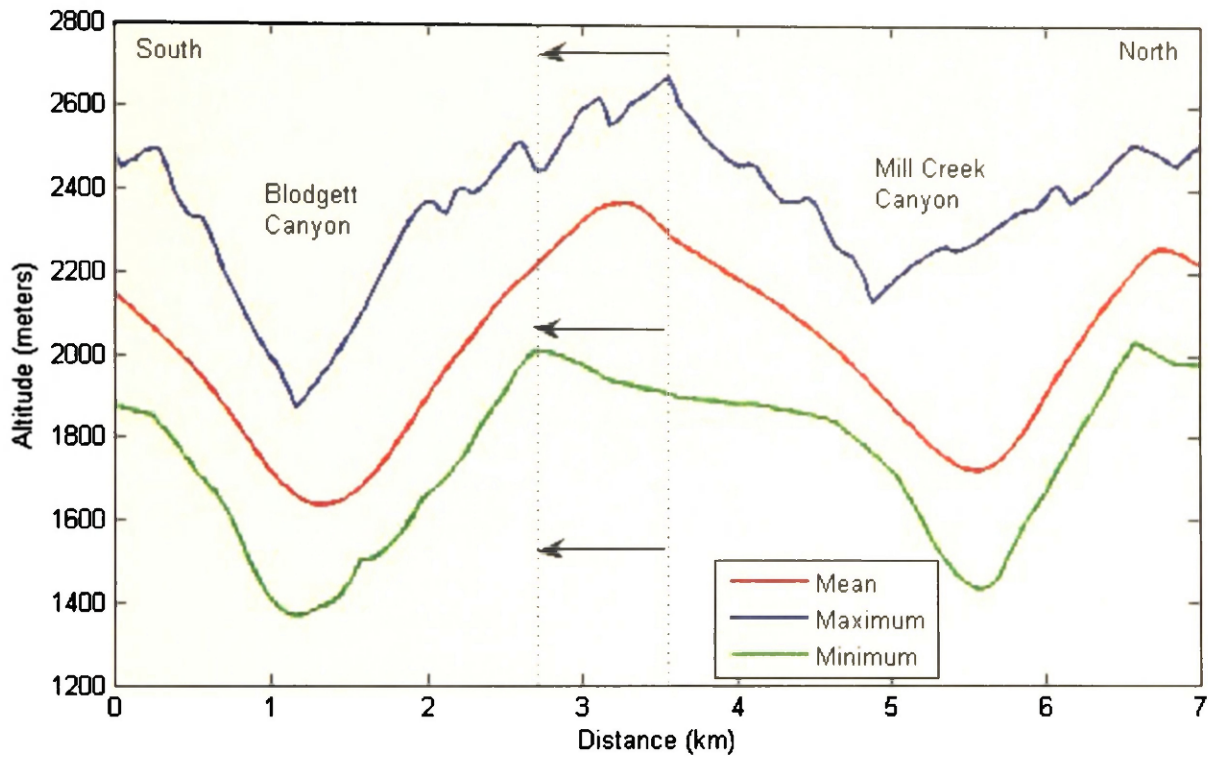


**Figure 2. Cross-sectional profile extracted from a rectangular swath (8 km wide, 12 km long) encompassing Blodgett and Mill Creek Canyons. Maximum elevations represent the locations of sub-basin interfluvies that display similar slopes on each side of the canyons. Minimum elevations represent the locations of sub-basin bottoms and show the effects of gradational processes for each slope. Dashed lines and arrows illustrate the southward migration of the divide. North-facing slopes have been “flattened” due to cirque formation and expansion.**



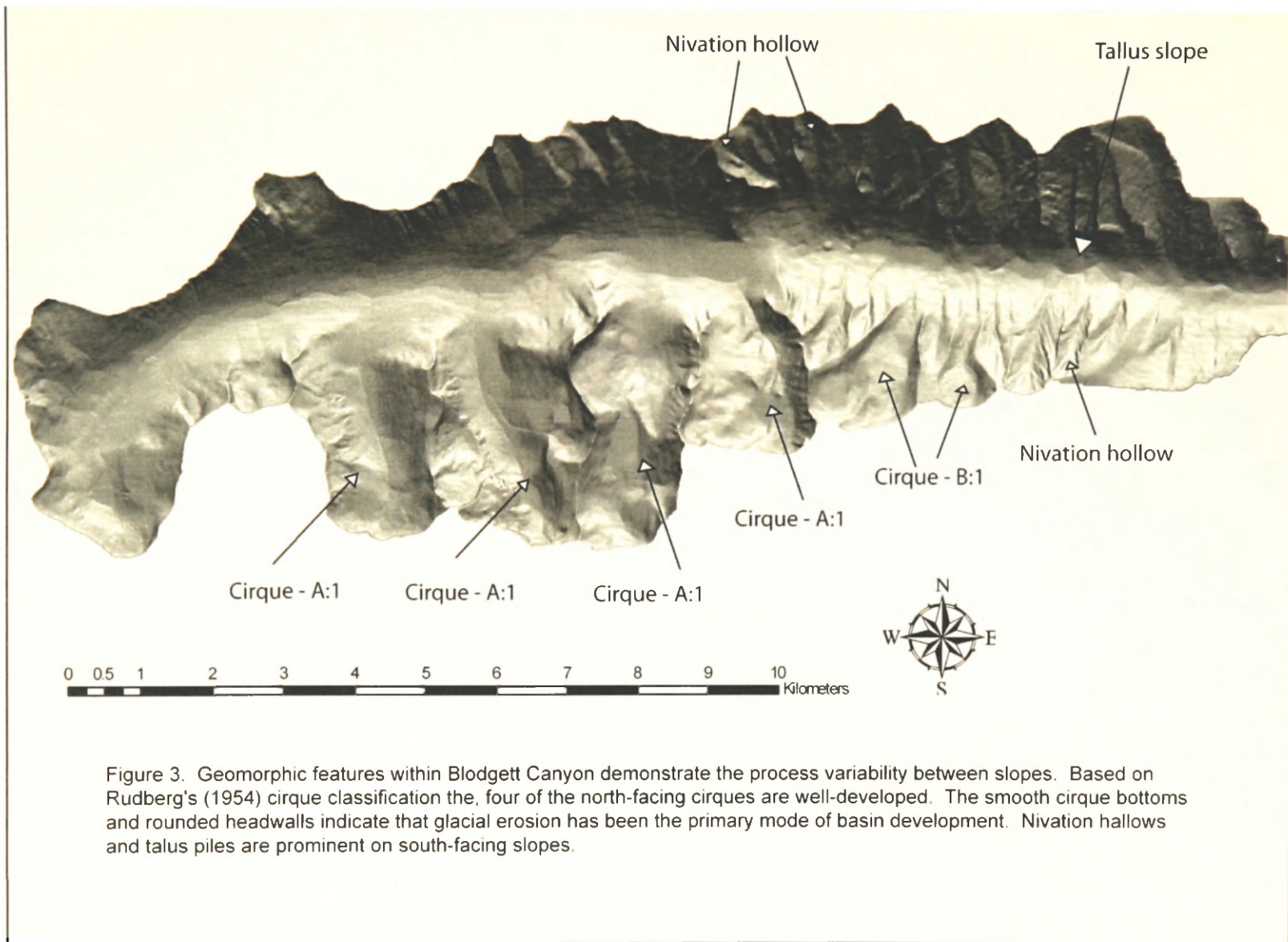
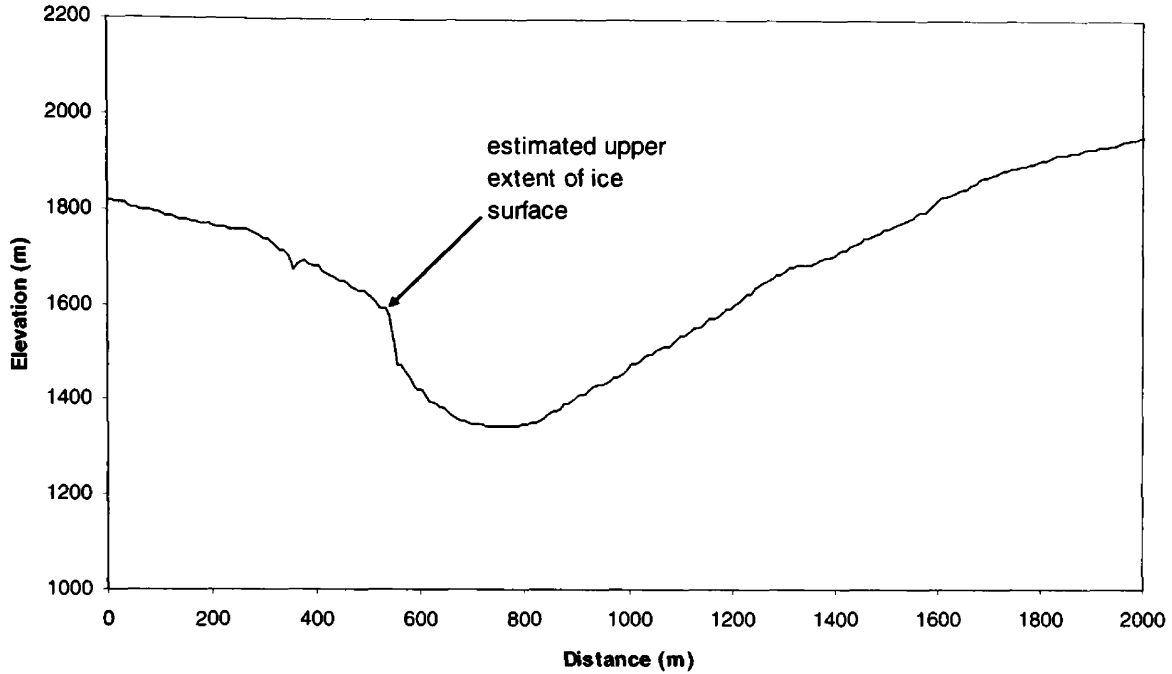
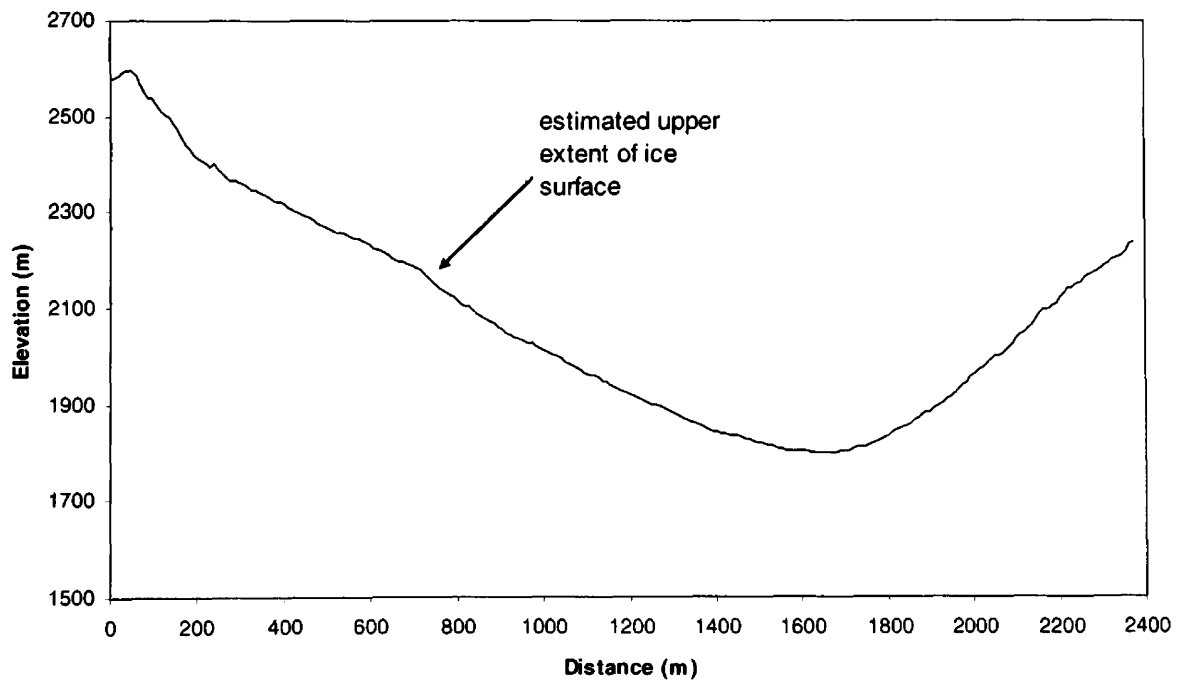


Figure 3. Geomorphic features within Blodgett Canyon demonstrate the process variability between slopes. Based on Rudberg's (1954) cirque classification the, four of the north-facing cirques are well-developed. The smooth cirque bottoms and rounded headwalls indicate that glacial erosion has been the primary mode of basin development. Nivation hollows and talus piles are prominent on south-facing slopes.



**Figure 4. Fred Burr valley cross-section derived along a truncated spur perpendicular to the main valley (2.2 km up-canyon). A prominent slope break exists on the south-facing slope (left-hand portion of graph) represents the top of the glacial trough and the top of the ice surface.**



**Figure 5. Fred Burr valley cross-section derived along a truncated spur perpendicular to the main valley (12.0 km up-canyon). The break in slope located at approximately 2200 m is used to interpolate the modeled ice surface.**



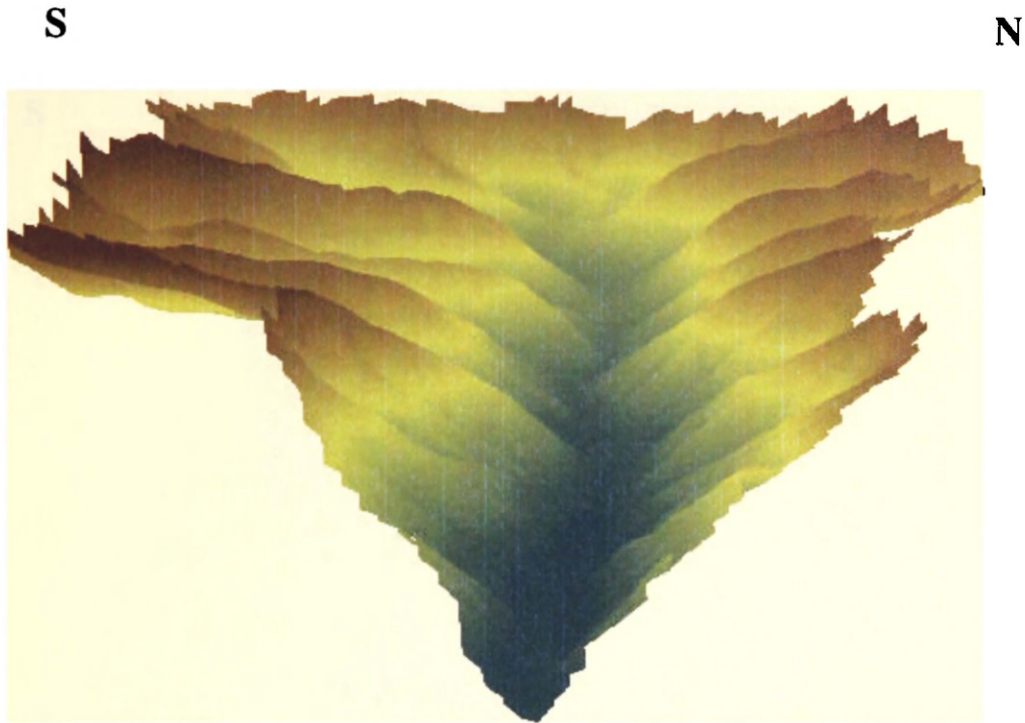


**Figure 6. Sub-ridgeline relief was calculated using a spline surface fitted between north- and south-facing interfluves. This figure displays prominent interfluves in Kootenai Creek Canyon. Points were marked along the interfluves and used to create the spline surface.**

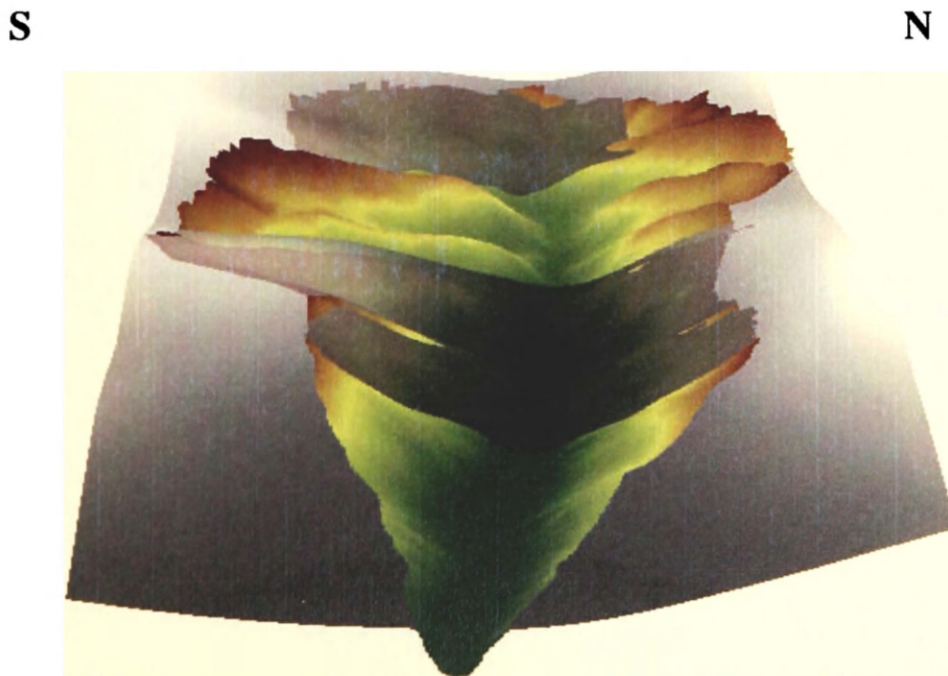


**Figure 7. Spline surface fitted between interfluve points for Kootenai Creek Canyon. The spline interpolation provides a benchmark from which we can calculate the amount of material eroded. The cut-fill command was used in ArcMap to calculate the north- and south-facing volume removed below the spline surface.**

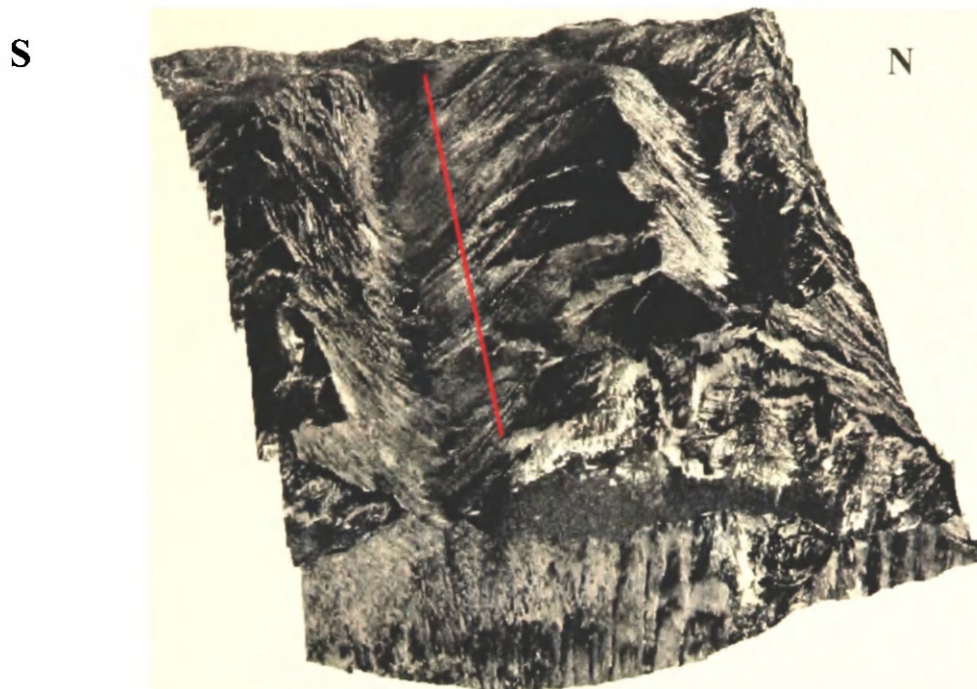


**Figure 8. Fred Burr Canyon with an orthophoto overlain on the 10 m USGS DEM. The red line shows the approximate elevation of the trimline on the north-facing slopes.**

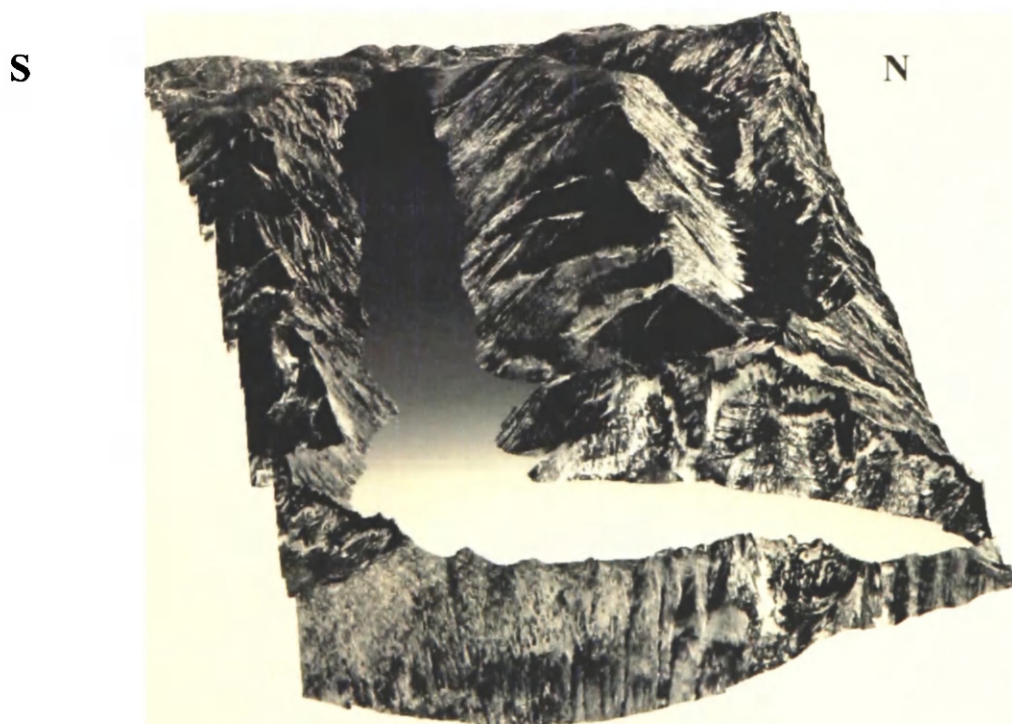


**Figure 9. The modeled ice surface for Fred Burr Canyon sloping downward toward the Bitterroot Valley. A spline interpolation was fitted between points to derive the modeled glacier. The surface closely matches the trimline shown in Figure 8. Slope, relief, and hypsometry analyses were performed on terrain above the surface.**

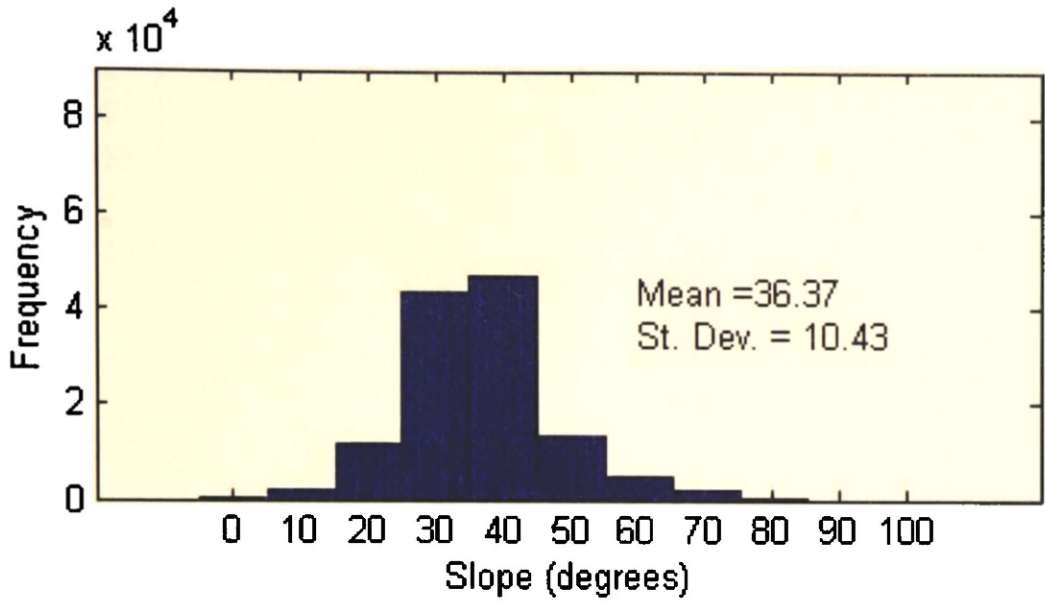


**Figure 10.** A histogram showing the distribution of slope calculations for Blodgett Canyon. The values represent composite slope calculations for the south-facing side of the canyon.

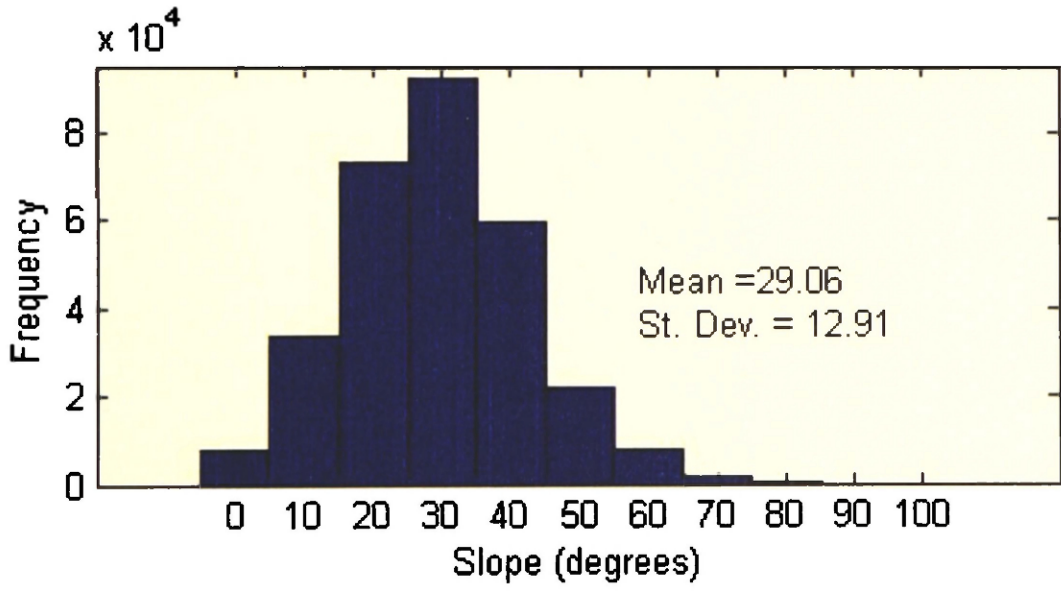


**Figure 11.** Slope frequency distributions for the north-facing side of Blodgett Canyon. The mean slope angle on north-facing slopes is 7° lower than on the south-facing slopes. Standard deviation is 2.5° greater for north-facing slopes suggesting that greater variability exists within glaciated areas.

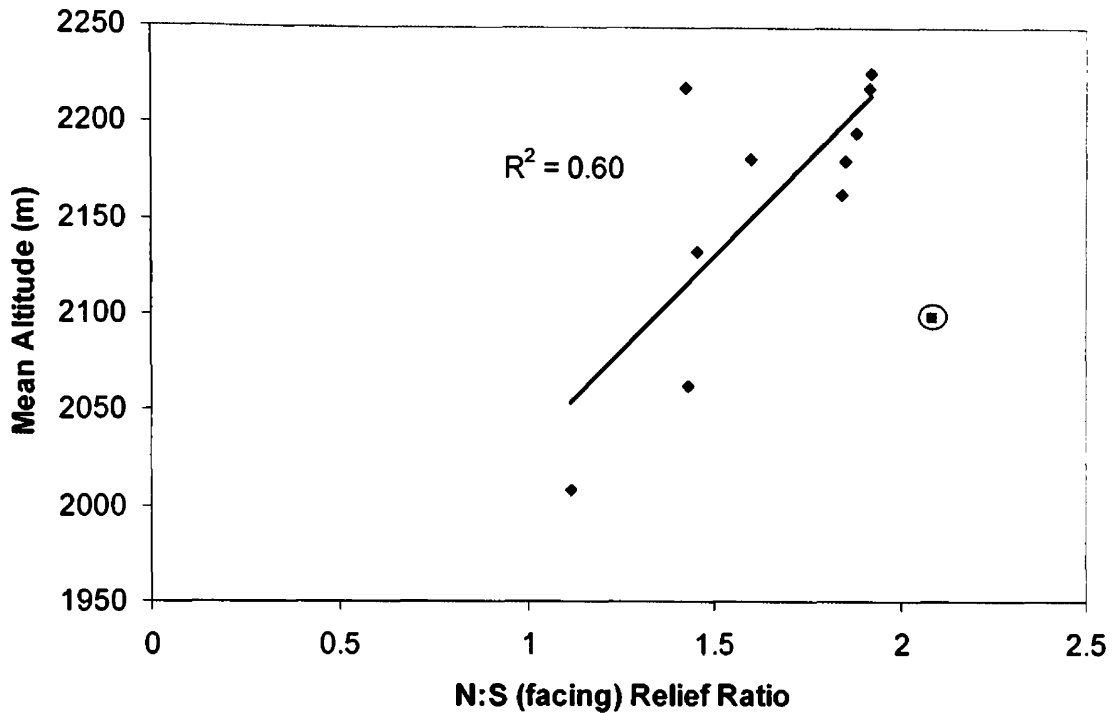


**Figure 12.** The difference in relief production increases for canyons in the southern Bitterroot Range where higher altitudes exist ( $R^2=0.60$ ). One outlier, Lost Horse Canyon, is removed from the regression because the south-facing analyzed slope only extends half the distance of the canyon (see Plate 9).

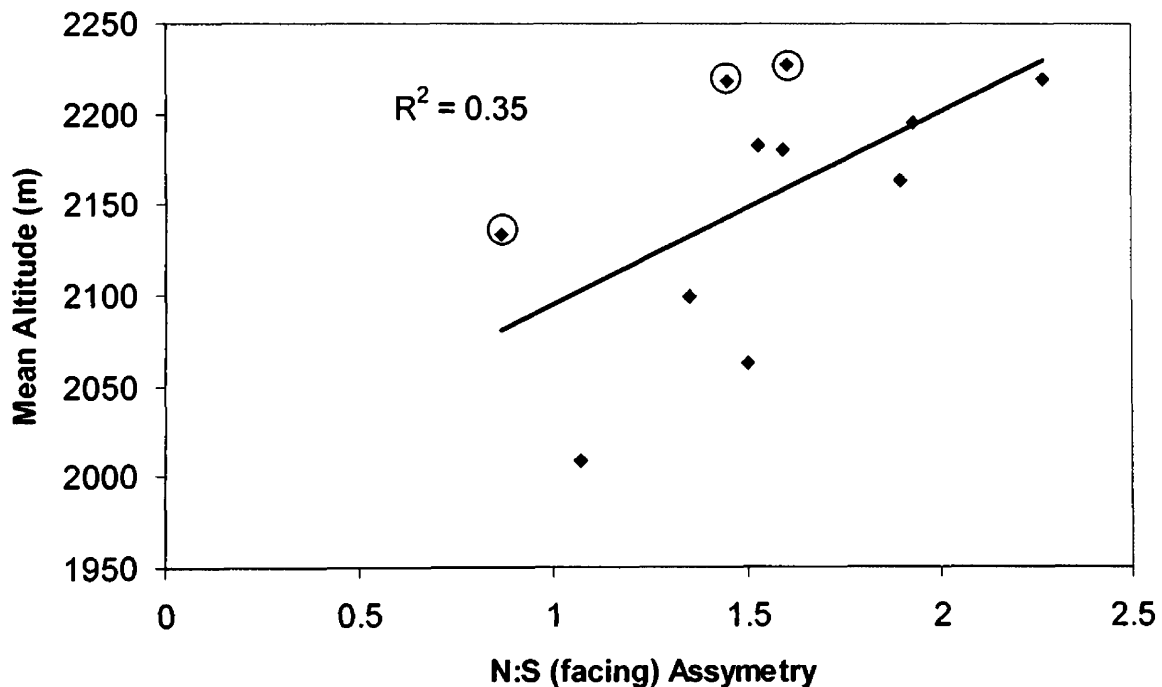
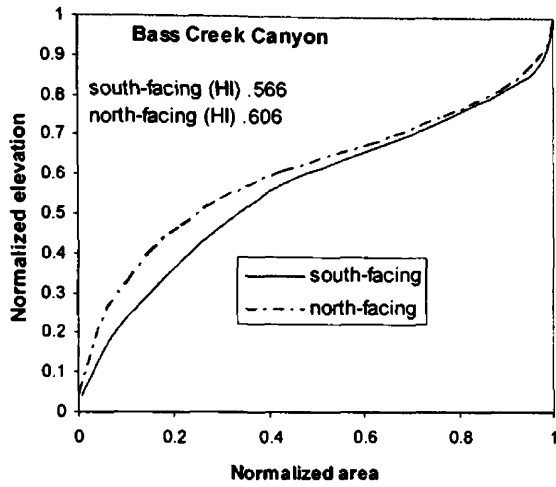
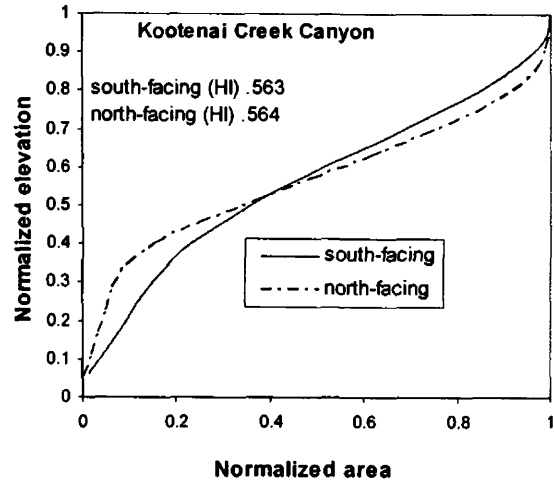


**Figure 13.** A modest correlation ( $R^2=0.35$ ) exists when plotting mean altitude versus canyon asymmetry. A better correlation ( $R^2=0.70$ ) is obtained by omitting three outliers: Bass Creek, Canyon Creek, and Sawtooth-Roaring Lion Canyons (justification for removing these outliers is provided in the discussion). The correlation supports the hypothesis that asymmetry is a product of differential processes as glacial erosion is enhanced above the paleo-ELAs.

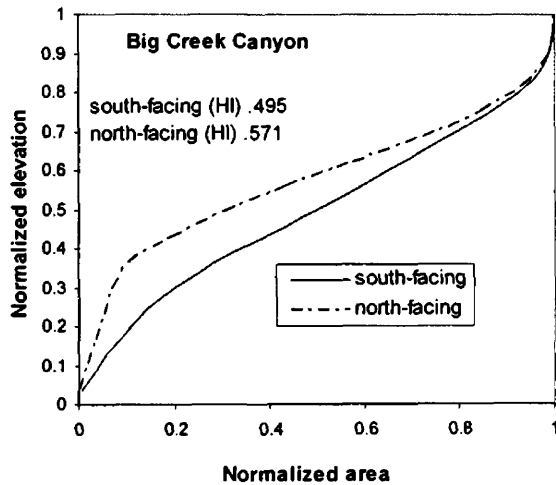
14 a



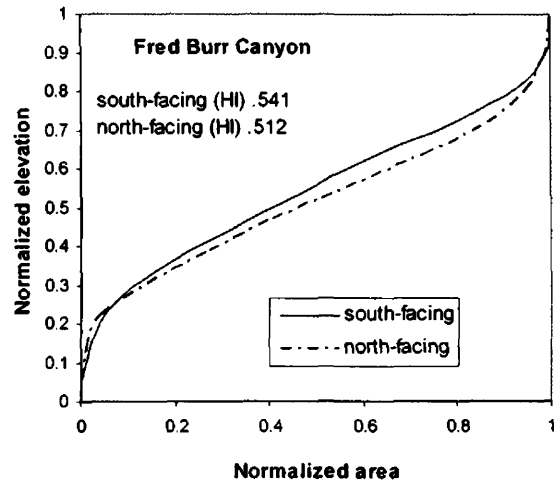
14 b



14 c



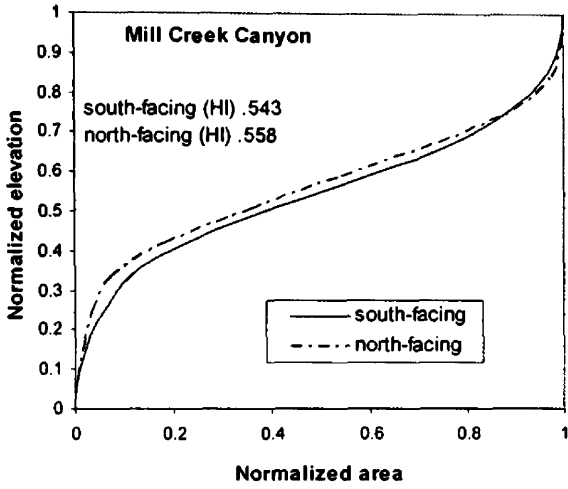
14 d



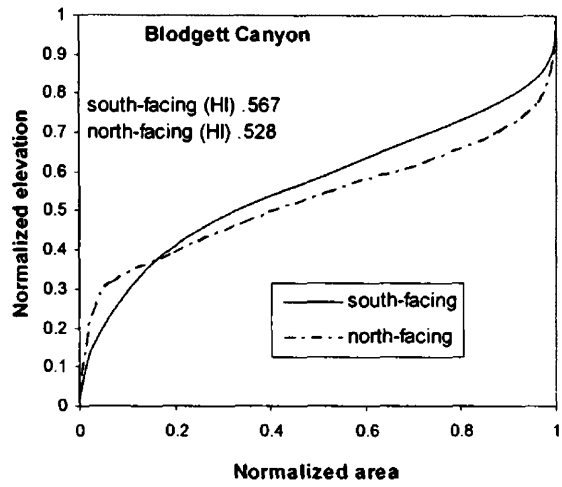
**Figures 14a - k. Hypsometric curves for each of the canyons display the effects of glacial erosion on elevation distributions. North-facing slopes generally show a shift in distribution towards lower altitudes suggesting that sediment transport mechanisms have more efficiently moved material on glaciated slopes.**



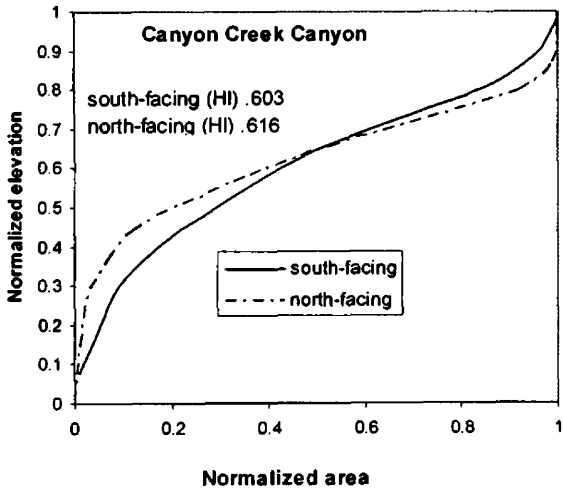
14 e



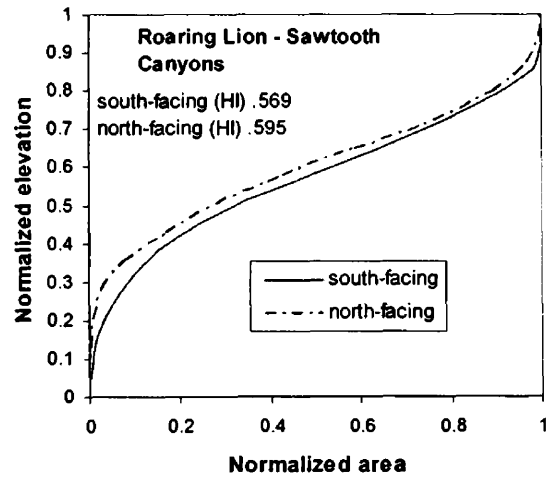
14 f



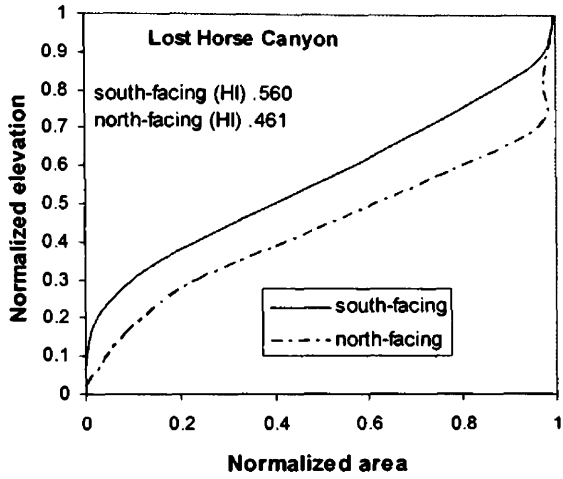
14 g



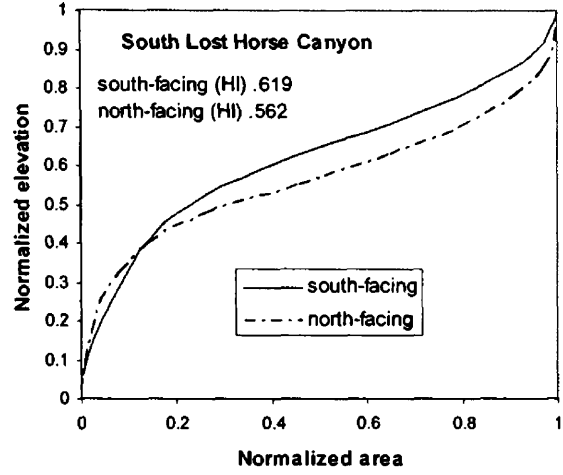
14 h



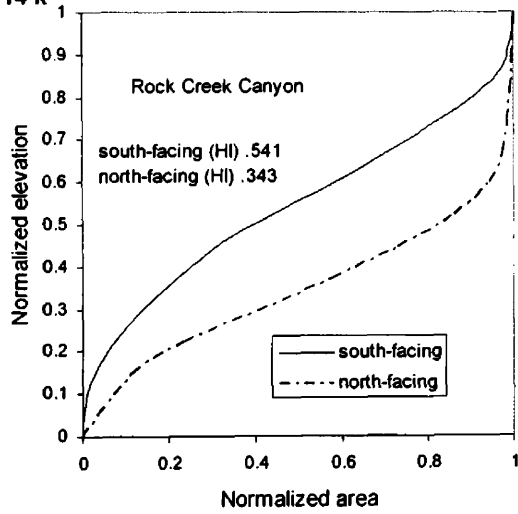
14 i



14 j



14 k



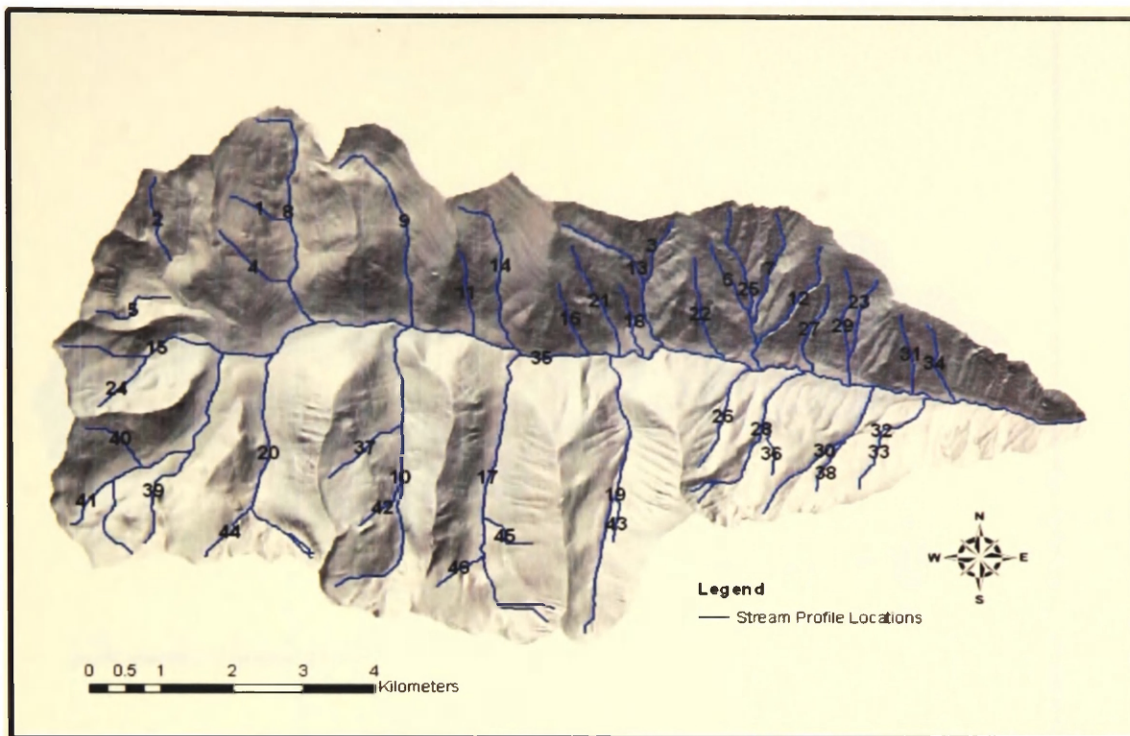


**Figure 15. Longitudinal profiles were extracted for tributary streams in Kootenai Canyon using an AML script. Profiles starting at the similar up-canyon distance are compared for each slope (e.g. #9 and #10).**

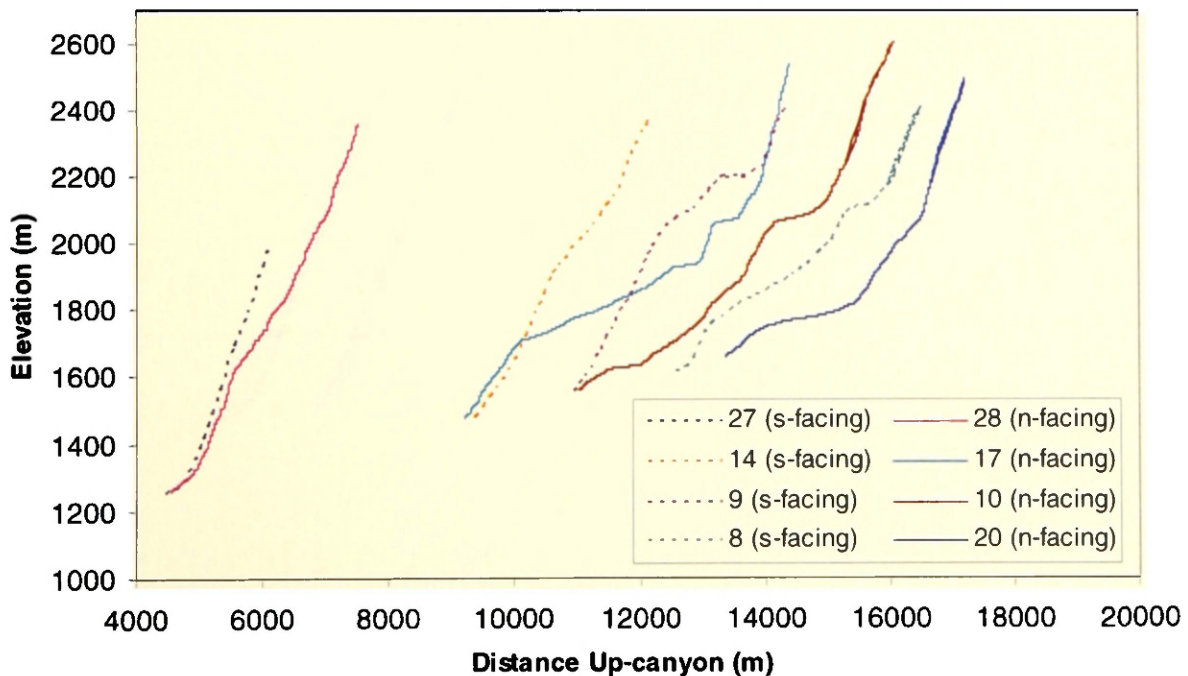


**Figure 16. Graph showing longitudinal profiles for both slopes in Kootenai Canyon. South-facing tributary profiles are generally straight except near the upper reaches of the canyon. North-facing profiles show greater concavity in the up-canyon direction and an increasing step-wise profile characteristic of glaciated terrain.**



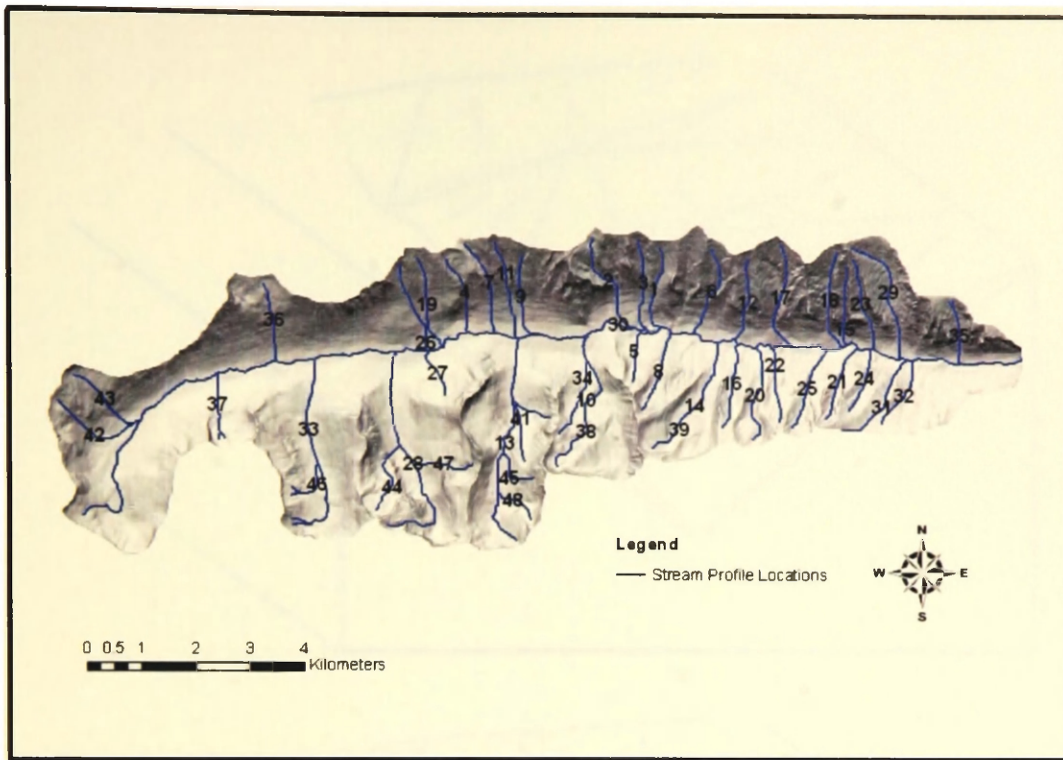


**Figure 17. Tributary longitudinal profiles extracted within Blodgett Canyon.**

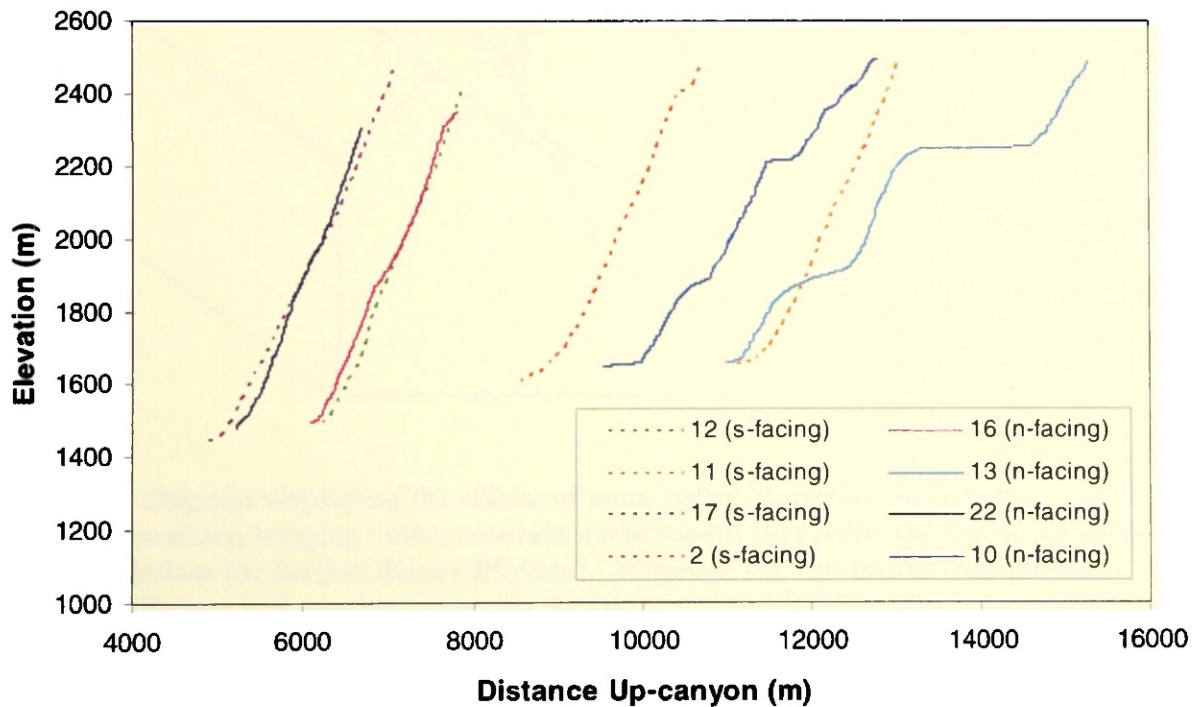
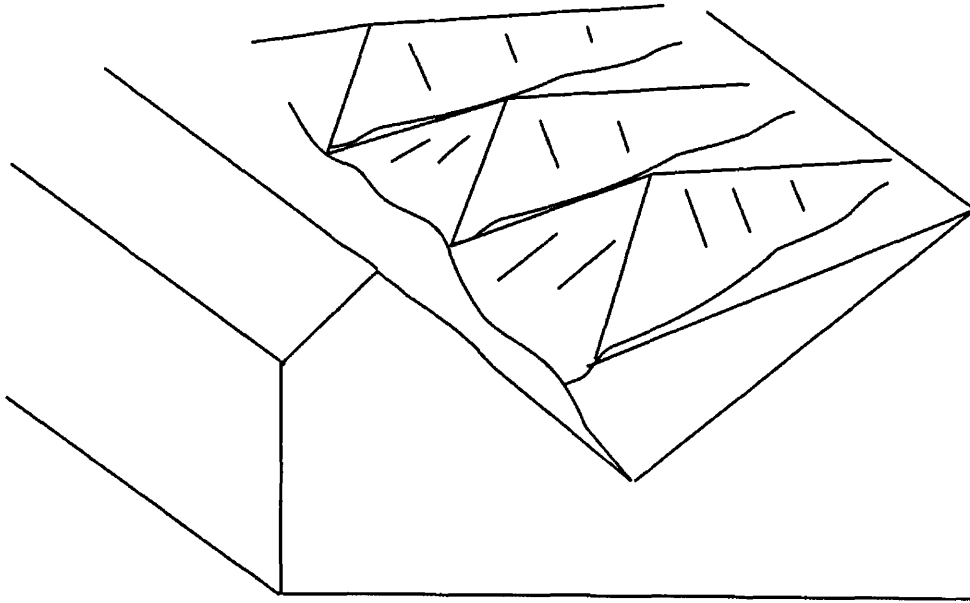


**Figure 18. Blodgett Canyon longitudinal profile comparison showing north-facing drainages with an increasingly step-wise form above paleo-ELAs. The change in form between profiles 10 and 13 demonstrates a prominent increase in headwall retreat.**

(A)



(B)

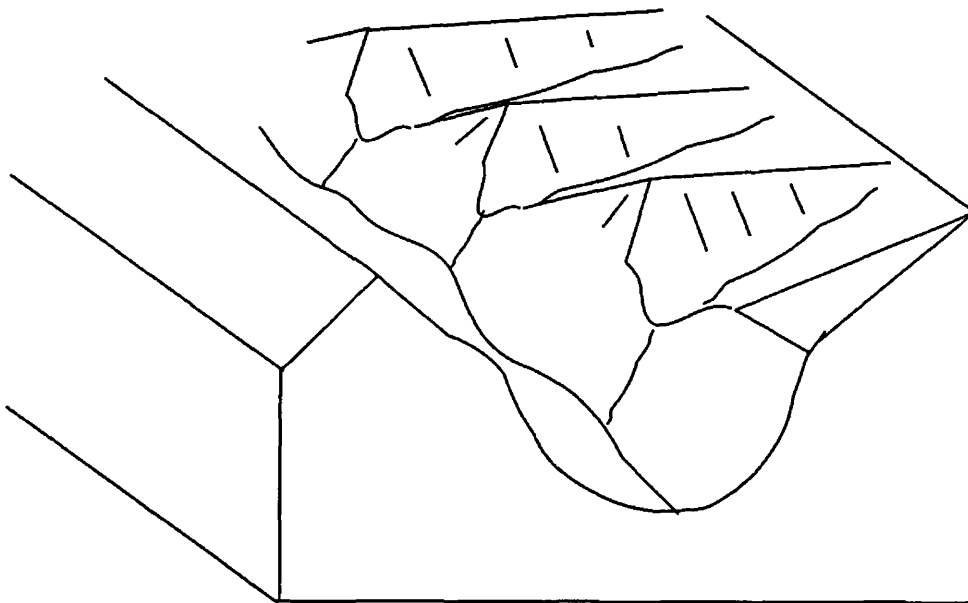


**Figure 19. A diagram displaying the effects of main valley glaciation on tributary fluvial basins. The resulting hanging valleys contain a knickpoint that shifts the fluvial network into disequilibrium (or further disequilibrium). Although the sub-basins' pre-glacial maxima equilibrium is dependent upon the timing of normal faulting along the range front (faulting along the Bitterroot Fault would impose major base level changes), the widening of the main valley during glacial maxima will nonetheless propagate a knickpoint. (A) Pre-glacial morphology, (B) Post-glacial morphology**

**Table 1. Summary of Shear Stress Calculations**

<b>Canyon</b>	<b>Average ice thickness (m)</b>	<b>Average Shear stress (<math>\tau_b</math>) N/m<sup>2</sup></b>
<i>Bass Creek</i>	231	1.54E+05
<i>Big Creek</i>	238	1.14E+05
<i>Blodgett</i>	318	1.42E+05
<i>Canyon Creek</i>	192	1.13E+05
<i>Fred Burr</i>	268	1.28E+05
<i>Kootenai</i>	303	1.97E+05
<i>Lost Horse</i>	508	7.12E+04
<i>Mill Creek</i>	334	1.51E+05
<i>Roaring Lion</i>	294	1.11E+05
<i>Rock Creek</i>	487	1.33E+05
<i>Sawtooth</i>	346	7.79E+04
<i>South Lost Horse</i>	299	9.97E+04
mean:	318	1.24E+05

**Table 2. Slope Analysis Results**

<b>Watershed</b>	<b>N-facing</b>	<b>N-facing</b>	<b>S-facing</b>	<b>S-facing</b>
	<b>Average slope (degree)</b>	<b>Standard deviation (degree)</b>	<b>Average slope (degree)</b>	<b>Standard deviation (degree)</b>
<i>Bass Creek</i>	31.5	11.4	35.4	9.6
<i>Kootenai Creek</i>	30.8	10.9	33.6	8.2
<i>Big Creek</i>	29.3	11.7	30.5	9.0
<i>Fred Burr</i>	28.8	10.9	38.2	10.5
<i>Mill Creek</i>	29.0	11.5	36.6	11.6
<i>Blodgett</i>	29.1	12.9	36.5	10.4
<i>Canyon Creek</i>	25.7	12.1	28.6	10.8
<i>Sawtooth-Roaring Lion</i>	26.8	12.0	35.7	8.3
<i>Lost Horse</i>	22.4	11.1	31.3	6.9
<i>South Lost Horse</i>	26.6	12.6	37.4	9.6
<i>Rock Creek</i>	25.2	13.7	26.8	11.1
Average:	27.7	11.9	33.7	9.6

**Table 3. Geophysical Relief Results**

<b>Watershed</b>	<b>S-facing Volume (m<sup>3</sup>)</b>	<b>N-facing Volume (m<sup>3</sup>)</b>	<b>S-facing Area (m<sup>2</sup>)</b>	<b>N-facing Area (m<sup>2</sup>)</b>	<b>S-facing Vol./Area ratio (m)</b>	<b>N-facing Vol./Area ratio (m)</b>
<i>Bass Creek</i>	1.3E+09	2.3E+09	9.9E+06	1.2E+07	128	186
<i>Kootenai Creek</i>	2.2E+09	1.0E+10	1.2E+07	3.7E+07	190	272
<i>Big Creek</i>	5.0E+09	1.2E+10	1.9E+07	4.1E+07	267	298
<i>Fred Burr</i>	8.7E+08	5.7E+09	7.3E+06	2.5E+07	120	227
<i>Mill Creek</i>	7.8E+08	4.7E+09	6.8E+06	2.2E+07	114	210
<i>Blodgett</i>	1.5E+09	7.1E+09	1.2E+07	2.9E+07	132	244
<i>Canyon Creek</i>	1.7E+08	7.8E+08	3.3E+06	7.8E+06	53	101
<i>Sawtooth-Roaring Lion</i>	1.4E+09	7.3E+09	1.3E+07	3.5E+07	109	209
<i>Lost Horse</i>	3.8E+08	6.7E+09	4.9E+06	2.3E+07	89	185
<i>South Lost Horse</i>	8.9E+08	5.5E+09	6.3E+06	2.7E+07	142	203
<i>Rock Creek</i>	3.3E+09	1.5E+10	1.8E+07	4.9E+07	186	297
<i>mean:</i>	1.6E+09	7.0E+09	1.0E+07	2.8E+07	139	221

**Table 4. Asymmetry and Hypsometry Results**

<b>Watershed</b>	<b>North / South Stream-ridgeline length ratio</b>	<b>Mean Elevation (m)</b>	<b>N-facing Hypsometric integral</b>	<b>S-facing Hypsometric integral</b>
<i>Bass Creek</i>	0.86	2133.60	0.606	0.566
<i>Kootenai Creek</i>	1.50	2062.76	0.564	0.563
<i>Big Creek</i>	1.07	2008.82	0.571	0.495
<i>Fred Burr</i>	1.93	2195.05	0.512	0.541
<i>Mill Creek</i>	1.90	2163.33	0.558	0.543
<i>Blodgett</i>	1.59	2180.56	0.528	0.567
<i>Canyon Creek</i>	1.45	2218.37	0.616	0.603
<i>Sawtooth-Roaring Lion</i>	1.60	2226.56	0.595	0.569
<i>Lost Horse</i>	1.35	2098.95	0.461	0.560
<i>South Lost Horse</i>	2.27	2218.88	0.562	0.619
<i>Rock Creek</i>	1.53	2181.96	0.343	0.541
<i>mean:</i>	1.55	2153.53	0.538	0.561



**Plate 2. Sleeping Child Canyon (slight asymmetry favoring south-facing slope)**



**Plate 3. Bedrock Reach along Blodgett Creek**





**Plate 4. Step-pool Reach along Kootenai Creek  
(Photo by Dick Gibson)**



**Plate 5. Cascading Reach along Blodgett Creek**



**Plate 6. Pool-riffle Reach along Bass Creek  
(Photo by Dick Gibson)**



**Plate 7. North-South Trending Fractures in  
Sweathouse Canyon**





**Plate 8. Truncated Spur in Bass Creek Canyon  
(Photo by Dick Gibson)**



## **Appendix**

### **USGS 10-meter DEM Metadata**

Metadata for 7.5-minute Digital Elevation Models (DEMs)

- 10 meter resolution

These metadata describe the 7.5-minute digital elevation models with a resolution of 10 meters.

-----  
-

Table of Contents

Identification\_Information  
Data\_Quality\_Information  
Spatial\_Data\_Organization\_Information  
Spatial\_Reference\_Information  
Entity\_and\_Attribute\_Information  
Distribution\_Information  
Metadata\_Reference\_Information

-----  
-

Identification\_Information:

Citation:

Citation\_Information

Originator: U.S. Geological Survey

Publication\_Date: 199807

Title: 7.5 minute Digital Elevation Models

Geospatial\_Data\_Presentation\_Form: map

Publication\_Information:

Publication\_Place: Menlo Park, CA

Publisher: U. S. Geological Survey

Description:

Abstract:

Digitntains a series of elevations ordered from south to north with the order of the columns from west to east. The DEM is formatted as one ASCII header record (A- record), followed by a series of profile records (B- records) each of which include a short B-record header followed by a series of ASCII integer elevations per each profile. The last physical record of the DEM is an accuracy record (C-record).

7.5-minute DEM (10- by 10-m data spacing, cast on Universal Transverse Mercator (UTM) projection). Provides coverage in 7.5- by 7.5-minute blocks. Each product provides the same coverage as a standard USGS 7.5-minute quadrangle without over edge.

Purpose:

DEM's can be used as source data for digital orthophotos, and, as layers in geographic information systems, for earth science analysis. DEM's can also serve as tools for volumetric analysis, for site location of towers, or for drainage basin delineation. These data were collected as part of the National Mapping Program.

Supplemental\_Information:

7.5-minute DEMs have rows and columns which vary in length and are staggered. The UTM bounding coordinates form a quadrilateral (no two sides are parallel to each other), rather than a rectangle. The user will need to pad out the uneven rows and columns with blanks or flagged data values, if a rectangle is required for the user's application. Some software vendors have incorporated this function into their software for input of standard formatted USGS DEMs.

Time\_Period\_of\_Content:

Time\_Period\_Information:

Range\_of\_Dates/Times:

Beginning\_Date: 197907

Ending\_Date: present

Currentness\_Reference: ground condition

Status

Progress: In work

Maintenance\_and\_Update\_Frequency: Irregular

Spatial\_Domain

Bounding\_Coordinates:

West\_Bounding\_Coordinate: -124.7333

East\_Bounding\_Coordinate: -067.9500

North\_Bounding\_Coordinate: 49.3833

South\_Bounding\_Coordinate: 24.5333

Keywords:

Theme:

Theme\_Keyword\_Thesaurus: none

Theme\_Keyword: DEM

Theme\_Keyword: digital elevation model

Theme\_Keyword: digital terrain model

Theme\_Keyword: hypsography

Theme\_Keyword: altitude

Theme\_Keyword: height

Theme\_Keyword: contour line

Theme\_Keyword: digital contours

Place:

Place\_Keyword\_Thesaurus:

U.S. Department of Commerce, 1977, Countries, dependencies,  
areas of special sovereignty, and their principal  
administrative divisions

(Federal Information Processing Standard 10-3): Washington,  
D.C.,

National Institute of Standards and Technology.

Place\_Keyword: US

Place\_Keyword\_Thesaurus:

U.S. Department of Commerce, 1987, Codes for the identification  
of the States, the District of Columbia and the outlying areas  
of

The United States, and associated areas

(Federal Information Processing Standard 5-2): Washington, D.  
C.,

National Institute of Standards and Technology.

Place\_Keyword: FIPS code of State or Province

Place\_Keyword\_Thesaurus:

U.S. Department of Commerce, 1990, Counties and equivalent  
entities of The United States, its possessions, and associated  
areas

(Federal Information Processing Standard 6-4): Washington,  
D.C.

National Institute of Standards and Technology.

Place\_Keyword: FIPS code for county or counties.

Access\_Constraints: None

Use\_Constraints:

None. Acknowledgement of the U.S. Geological Survey would be appreciated in products derived from these data.

#### Data\_Quality\_Information

Attribute\_Accuracy:

Attribute\_Accuracy\_Report:

The accuracy of a DEM is dependent upon the level of detail of the source and the grid spacing used to sample that source. The primary limiting factor for the level of detail of the source is the scale of the source materials. The proper selection of grid spacing determines the level of content that may be extracted from a given source during digitization.

Logical\_Consistency\_Report:

The fidelity of the relationships encoded in the data structure of the DEM are automatically verified using a USGS software program upon completion of the data production cycle. The test verifies full compliance to the DEM specification.

Completeness\_Report:

The DEM is visually inspected for completeness on a DEM view and edit system for the purpose of performing a final quality control and if necessary edit of the DEM. The physical format

of each digital elevation model is validated for content completeness and logical consistency during production quality control and prior to archiving in the National Digital Cartographic Data Base.

Due to the variable orientation of the quadrilateral in relation to the Universal Transverse Mercator (UTM) projection grid, profiles that pass within the bounds of the DEM quadrilateral, may be void of elevation grid points, and are not represented in the DEM. This condition occurs infrequently and is always the first or last profile of the dataset.

Level 2 DEM: Level 2 DEM's may contain void areas due to interruptions to contours in the source graphic or DLG. Void area elevation grid posts are assigned the value of -32,767. In addition, suspect elevation areas may exist in the DEM but are not specifically identified. Suspect areas can be located on the source graphic as a "disturbed surface, " symbolized by contours overprinted with photorevised or other surface patterns.

Positional\_Accuracy:

Horizontal\_Positional\_Accuracy:

Horizontal\_Positional\_Accuracy\_Report:

The horizontal accuracy of the DEM is expressed as an estimated root mean square error (RMSE). The estimate of the RMSE is based upon horizontal accuracy tests of the DEM source materials which are selected as equal to or less than intended horizontal RMSE error of the DEM.

The testing of horizontal accuracy of the source materials is accomplished by comparing the planimetric (X and Y) coordinates of well-defined ground points with the coordinates of the same points as determined from a source of higher accuracy.

Quantitative\_Horizontal\_Positional\_Accuracy\_Assessment:

Horizontal\_Positional\_Accuracy\_Value: RMSE of the DEM.

Horizontal\_Positional\_Accuracy\_Explanation:

Digital elevation models meet horizontal National Map Accuracy Standards (NMAS) accuracy requirements.

Vertical\_Positional\_Accuracy:

Vertical\_Positional\_Accuracy\_Report:

The vertical RMSE statistic is used to describe the vertical accuracy of a DEM, encompassing both random and systematic errors introduced during production of the data. The RMSE is encoded in element number 5 of record C of the DEM.

Accuracy is computed by a comparison of linear interpolated elevations in the DEM with corresponding known elevations. Test points are well distributed, representative of the terrain, and have true elevations with accuracies well within the DEM accuracy criteria. Acceptable test points include, in order of preference: field control, aerotriangulated test points, spot elevations, or points on contours from existing source maps with appropriate contour interval. A minimum of



28 test points per DEM is required to compute the RMSE, which is composed of a single test using 20 interior points and 8 edge points. Edge points are those which are located along, at, or near the quadrangle neatlines and are deemed by the editor to be useful to evaluating the accuracy of the edge of the DEM. Collection of test point data and comparison of the DEM with the quadrangle hypsography are conducted by the quality control units within the USGS.

There are three types of DEM vertical errors; blunder, systematic and random. These errors are reduced in magnitude by editing but cannot be completely eliminated. Blunder errors are those errors of major proportions and are easily identified and removed during interactive editing. Systematic errors are those errors that follow some fixed pattern and are introduced by data collection procedures and systems. These error artifacts include: vertical elevation shifts, misinterpretation of terrain surface due to trees, buildings and shadows, and fictitious ridges, tops, benches or striations. Random errors result from unknown or accidental causes.

DEM's are edited to correctly depict elevation surfaces that correspond to water bodies of specified size.

Level 2 DEM: A vertical RMSE of one-half of the contour interval, determined by the source map, is the maximum permitted. Systematic errors may not exceed one contour interval, determined by the source map, is the maximum permitted. Systematic errors may not exceed one contour interval specified by the source graphic. Level 2 DEMs have been processed or smoothed for consistency and edited to remove identifiable systematic errors.

Quantitative\_Vertical\_Positional\_Accuracy\_Assessment:

Vertical\_Positional\_Accuracy\_Value:

Vertical\_Positional\_Accuracy\_Explanation: RMSE of the DEM.

Lineage:

Source\_Information:

Source\_Citation:

Citation\_Information:

Originator: U.S. Geological Survey

Publication\_Date:

Title: digital contour lines

Geospatial\_Data\_Presentation\_Form: map

Publication\_Information:

Publication\_Place: Reston, VA

Publisher: U.S. Geological Survey

Type\_of\_Source\_Media: magnetic tape

Source\_Time\_Period\_of\_Content:

Time\_Period\_Information:

Range\_of\_Dates/Times:

Beginning\_Date: 197907

Ending\_Date: present

Source\_Currentness\_Reference: ground condition

Source\_Citation\_Abbreviation: CONTOUR1

Source\_Contribution:

regular  
hypsographic vector information which is interpolated to  
grid posts to form DEM grids in 10- by 10- meter UTM data  
spacing  
within the 7.5 minute DEM bounds.

Source\_Information:

Source\_Citation:

Citation\_Information:

Originator: U.S. Geological Survey

Publication\_Date:

Title: photo ID number

Geospatial\_Data\_Presentation\_Form: remote-sensing image

Publication\_Information:

Publication\_Place: Reston, VA

Publisher: U.S. Geological Survey

Type\_of\_Source\_Media: transparency

Source\_Time\_Period\_of\_Content:

Time\_Period\_Information:

Range\_of\_Dates/Times:

Beginning\_Date: various

Ending\_Date: various

Source\_Currentness\_Reference: ground condition

Source\_Citation\_Abbreviation: PHOTO1  
Source\_Contribution: elevation values

Source\_Information:

Source\_Citation:

Citation\_Information:

Originator: U.S. Geological Survey  
Publication\_Date: Unpublished material  
Title: project control  
Geospatial\_Data\_Presentation\_Form: map

Publication\_Information

Publication\_Place: Reston, VA  
Publisher: U.S. Geological Survey

Type\_of\_Source\_Media: magnetic tape

Source\_Time\_Period\_of\_Content:

Time\_Period\_Information

Range\_of\_Dates/Times:

Beginning\_Date: various  
Ending\_Date: various

Source\_Currentness\_Reference: ground condition

Source\_Citation\_Abbreviation: CONTROL1

Source\_Contribution: ground control points

Process\_Step:

Process\_Description:

Level 2 DEM: Level 2 DEM's are produced by  
converting 1:24,000-scale and 1:100,000-scale  
hypsography digital line graph (DLG) data to DEM

format or the DEM's are generated from vector data derived from scanned raster files of USGS 1:24,000-scale or 1:100,000-scale map series contour separates.

Level 3 DEM: Level 3 DEM's are created from DLG data that has been vertically integrated with all categories of hypsography, hydrography, ridge line, break line, drain files and all vertical and horizontal control networks. The production of level 3 DEMs requires a system of logic incorporated into the software interpolation algorithms that clearly differentiates and correctly interpolates between the various types of terrain, data densities and data distribution.

Water body editing: DEM surface areas corresponding to water bodies are flattened and assigned map specified or estimated surface elevations. Water body areas are defined as ponds, lakes, and reservoirs that exceed 0.5 inches at map scale and double line drainage that exceeds 0.25 inches at map scale. Water body shorelines are derived either from a hypsographic DLG or by interactive delineation from 1:24,000-scale or 1:100,000-scale USGS map series.

Edge matching and edge joining: DEM datasets within a project area (consisting of a number of

adjacent files) are edge match and edge join edited to assure terrain surface continuity between files. Edge matching is the process of averaging adjacent elevation values along common edges within a zone of approximately 5 row or column grid posts on both edges. When edge values exceed 3 elevation units difference, edge joining is performed. Edge joining is an extensive level of editing and requires editing elevation values internal to the DEM in order to create more accurate terrain representations by correcting the alignment of ridges and drains, and overall topographic shaping within an approximately 25-30 row or column grid post zone on both edges.

Quality control: DEM's are viewed on interactive editing systems to identify and correct blunder and systematic errors. DEM's are verified for physical format and logical consistency at the production centers and before archiving in the National Digital Cartographic Data Base (NDCDB) utilizing the Digital Elevation Model Verification System (DVS) software.

Source\_Used\_Citation\_Abbreviation: CONTOUR1, PHOTO1, CONTROL1

Process\_Date:

Spatial\_Data\_Organization\_Information

Direct\_Spatial\_Reference\_Method: raster

Raster\_Object\_Information:

Raster\_Object\_Type: grid cell

Row\_Count:

Column\_Count:

Spatial\_Reference\_Information:

Horizontal\_Coordinate\_System\_Definition:

Planar:

Grid\_Coordinate\_System:

Grid\_Coordinate\_System\_Name: Universal Transverse Mercator

Universal\_Transverse\_Mercator:

UTM\_Zone\_Number: 10-19

Transverse\_Mercator:

Scale\_Factor\_at\_Central\_Meridian: .99996

Longitude\_of\_Central\_Meridian: depends on zone

Latitude\_of\_Projection\_Origin: 0.0

False\_Easting: 500000

False\_Northing: 0.0

Planar\_Coordinate\_Information:

Planar\_Coordinate\_Encoding\_Method: row and column

Coordinate\_Representation:

Abscissa\_Resolution: 10

Ordinate\_Resolution: 10

Planar\_Distance\_Units: meters

Geodetic\_Model:

Horizontal\_Datum\_Name: North American Datum 1927

Ellipsoid\_Name: Clark 1866

Semi-major\_Axis: 6378206.4

Denominator\_of\_Flattening\_Ratio: 294.9787

Vertical\_Coordinate\_System\_Definition:

Altitude\_System\_Definition:

Altitude\_Datum\_Name: National Geodetic Vertical Datum of 1929

Altitude\_Resolution: 1

Altitude\_Distance\_Units: meters

Altitude\_Encoding\_Method:

explicit elevation coordinate included with horizontal coordinates

Entity\_and\_Attribute\_Information:

Overview\_Description:

Entity\_and\_Attribute\_Overview:

The digital elevation model is composed of a 6-character integer raster representing a gridded form of a topographic map hypsography overlay. Each raster entity contains a 6-character integer value between -32,767 to 32,768.

Entity\_and\_Attribute\_Detail\_Citation:



U.S. Department of the Interior, U.S. Geological Survey, 1992,  
Standards for digital elevation models: Reston, VA,

A hypertext version is available at:

<URL:  
[ftp://nmdpow9.er.usgs.gov/public/dem\\_html/standards\\_dem.html](ftp://nmdpow9.er.usgs.gov/public/dem_html/standards_dem.html)>

Softcopy in ASCII format is available at:

<URL: <ftp://nmdpow9.er.usgs.gov/public/demstnds/stdempt1.txt>>

<URL: <ftp://nmdpow9.er.usgs.gov/public/demstnds/stdempt2.txt>>

<URL: <ftp://nmdpow9.er.usgs.gov/public/demstnds/stdempt3.txt>>

Softcopy in WordPerfect format is available at:

<URL: <ftp://nmdpow9.er.usgs.gov/public/demstnds/stdempt1.wp5>>

<URL: <ftp://nmdpow9.er.usgs.gov/public/demstnds/stdempt2.wp5>>

<URL: <ftp://nmdpow9.er.usgs.gov/public/demstnds/stdempt3.wp5>>

Softcopy in PostScript format is available at:

<URL: <ftp://nmdpow9.er.usgs.gov/public/demstnds/stdempt1.ps>>

<URL: <ftp://nmdpow9.er.usgs.gov/public/demstnds/stdempt2.ps>>

<URL: <ftp://nmdpow9.er.usgs.gov/public/demstnds/stdempt3.ps>>

Distribution\_Information:

Distributor:

Contact\_Information:

Contact\_Organization\_Primary:

Contact\_Organization:

Earth Science Information Center, U.S. Geological Survey

Contact\_Address:

Address\_Type: mailing address

Address: 507 National Center

City: Reston

State\_or\_Province: Virginia

Postal\_Code: 22092

Contact\_Voice\_Telephone: 1 800 USA MAPS

Hours\_of\_Service: 0800-1600

Contact\_Instructions:

In addition to the address above there are other ESIC offices throughout the country. A full list of these offices is at:

<URL: [http://www-nmd.usgs.gov/esic/esic\\_index.html](http://www-nmd.usgs.gov/esic/esic_index.html)>

Resource\_Description: 7.5-minute digital elevation models

Distribution\_Liability:

Although these data have been processed successfully on a computer system at the U.S. Geological Survey, no warranty expressed or implied is made by the Geological Survey regarding the utility of the data on any other system, nor shall the act of distribution constitute any such warranty.

Standard\_Order\_Process:

Digital\_Form:

Digital\_Transfer\_Information:

Format\_Name: DEM

Format\_Information\_Content:

USGS standard DEM: The standard USGS  
DEM can be described as an ASCII formatted  
elevation file preceded by a metadata  
header file which consists of one 1024 byte  
ASCII record.

Transfer\_Size: 1

Digital\_Transfer\_Option:

Offline\_Option:

Offline\_Media:

Recording\_Format:

Compatibility\_Information: none

Fees:

The online copy of the data set (when available electronically)  
may  
be accessed without charge.

Metadata\_Reference\_Information:

Metadata\_Date: 199807

Metadata\_Contact:

Contact\_Information:

Contact\_Organization\_Primary:

Contact\_Organization: U.S. Geological Survey

Contact\_Address:

Address\_Type: mailing address

Address: 345 Middlefield Rd. MS 531

City: Menlo Park

State\_or\_Province: CA

Postal\_Code: 94025

Contact\_Voice\_Telephone: 650-329-4272

Metadata\_Standard\_Name: Content Standards for Digital Geospatial  
Metadata

Metadata\_Standard\_Version: 19940608